Ocean Modelling 194 (2025) 102490

Contents lists available at ScienceDirect

Ocean Modelling

journal homepage: www.elsevier.com/locate/ocemod

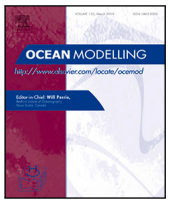

Analysis of the impact of vertical variation and temporal frequency of the chlorophyll forcing field on modelled temperature in the Mediterranean Sea and potential implications for regional climate projections

Yutong Zhang [a], Florence Sevault [b], Romain Pennel [c], Melika Baklouti [a,*]

[a] Aix-Marseille Université, Université de Toulon, CNRS, IRD, MIO UM 110, Campus de Luminy - OCEANOMED, CEDEX 09, Marseille, 13288, France
[b] CNRM, Université de Toulouse, Météo-France, CNRS, 42 avenue Gaspard Coriolis, Toulouse, 31057, France
[c] LMD/IPSL, École Polytechnique, Institut Polytechnique de Paris, ENS, PSL Research University, Sorbonne Université, CNRS, Rte de Saclay, Palaiseau, 91120, France

ARTICLE INFO

Keywords:
Forcing chlorophyll field
Biological feedback on physics
Light absorption
Ocean circulation model
Deep chlorophyll maximum
Mediterranean Sea

ABSTRACT

The urgency of climate change calls for the exploration of a variety of multi-forcing scenarios based on Shared Socio-economic Pathways. Ensuring the reliability of the climate projections is therefore an imperative prerequisite. In this paper, we examined the impact of the vertical variability and temporal frequency of the chlorophyll field used to force the NEMOMED12 ocean circulation model in the absence of a biogeochemical model on some key physical characteristics, mainly seawater temperature. Our analysis reveals that forcing by a chlorophyll field that is homogeneous in the vertical direction favours heat accumulation below the Deep Chlorophyll Maximum, leading to a positive temperature bias increasing with time. The extrapolation of the trend determined over the 11-year simulations leads to a bias in temperature as high as +1 °C after 100 years in the intermediate layer. Comparison with in situ data clearly shows that forcing the model with a realistically varying Chl field over the vertical allows the model to better represent temperature and avoid the presence of this bias. Additionally, we find that using the same chlorophyll field saved at different time frequencies, namely daily, monthly and monthly climatology, to force the NEMOMED12 model also creates temperature differences between simulations that increase with time, especially in the intermediate layer. The simulation forced by the daily chlorophyll is warmer in the surface layers than the two others, and we suggest that this is due to the asymmetric role of chlorophyll extremes on heat distribution. Finally, using a monthly chlorophyll climatology to force the NEMOMED12 ocean circulation model seems to be sufficient for physical modelling of the Mediterranean basin if the vertical variability of the Chl field is realistic.

1. Introduction

The urgency of climate change and its already perceptible effects on marine ecosystems (e.g. Hoegh-Guldberg and Bruno, 2010; Doney et al., 2012; Gattuso et al., 2018; Park et al., 2019) call for the exploration of a variety of multi-forcing scenarios based on the combination of socio-economic and greenhouse gases pathways (referred to as Shared Socio-economic Pathway, i.e. SSP scenarios in the latest IPCC report (IPCC, 2023)). This exploration is necessary not only to provide an envelope of climate projections but also to potentially identify scenarios that could be more resilient for marine ecosystems. These projections are based on earth system models that have been progressively enriched over time (e.g. Flato, 2011; Randall et al., 2018), most of which now include the main components involved in ecosystem functioning, i.e. atmospheric models (including aerosols dynamics and atmospheric chemistry), sea-ice models, continental models (including hydrology, land-use and vegetation dynamics), ocean circulation models, biogeochemical models (for the low-trophic levels of the marine food-web), and high-trophic level models.

However, the expensive computational costs that would be necessary to run fully-coupled versions of such model chains for the exploration of a large number of scenarios, have led to the production of only partially-coupled versions of the model chains (Wright and Davidson, 2020). A common practice is, therefore, to use a two-way coupling between atmosphere, land-surface, hydrology, and ocean circulation models, while the rest of the chain will be forced by the latter set of models to produce biogeochemical and biological projections (Menon et al., 2007; Flato, 2011). Such a practice implies that the chlorophyll (Chl) field that is used in the circulation model

* Corresponding author.
E-mail address: melika.baklouti@mio.osupytheas.fr (M. Baklouti).

https://doi.org/10.1016/j.ocemod.2024.102490
Received 27 September 2024; Received in revised form 3 December 2024; Accepted 17 December 2024
Available online 3 January 2025

for the absorption of shortwave irradiance by Chl pigments is not dynamically produced by the biogeochemical model, but is rather a pre-produced forcing field. Consequently, pragmatic solutions relying on several simplifying assumptions are often employed to generate this 3D Chl field, which can significantly impact the accuracy of the output of ocean circulation models.

Chlorophyll is indeed known to absorb shortwave photons, mainly in the red and blue long-waves (Rabinowitch, 1965), therefore impacting the vertical penetration of solar radiation into the ocean (Lin et al., 2008), the vertical distribution of heat balance (Lewis et al., 1983), air-sea heat fluxes (e.g. Oschlies, 2004; Wetzel et al., 2006), as well as water column stratification (Manizza et al., 2008). Numerous modelling studies have already investigated the feedback of phytoplankton Chl in the Pacific Ocean (Nakamoto et al., 2001; Lengaigne et al., 2007; Anderson et al., 2009; Tian et al., 2021), the Indian Ocean (Park and Kug, 2014; Ma et al., 2015; Gera et al., 2020), the Atlantic Ocean (Frouin et al., 2007; Hernandez et al., 2017), coastal regions (Nakamoto et al., 2000; Skákala et al., 2022), and the global ocean (e.g. Wetzel et al., 2006; Manizza et al., 2008; Gnanadesikan and Anderson, 2009; Patara et al., 2012; Asselot et al., 2021). Among the many results of these studies, it has been shown that the absorption of light by phytoplankton Chl results in a warming of the surface ocean (of the order of 0.2 to 2 °C) and a cooling of the subsurface (10–70 m) of the same order (Manizza et al., 2008; Löptien et al., 2009), leading to a reduction in the depth of the Mixed Layer (ML) of up to 20% (Lengaigne et al., 2007; Skákala et al., 2022). However, in upwelling areas, the presence of phytoplankton leads either to a warming of the sea surface in some studies (e.g. Lengaigne et al., 2007) or a cooling in others (e.g. Ma et al., 2015; Hernandez et al., 2017). Furthermore, a recent study by Skákala et al. (2022) also suggests that this biological feedback on physical characteristics could propagate to a depth of 200 m.

All this previous work contributed to the characterization of the biological feedback (through Chl concentration) on ocean physics. Considering the significant impact of this feedback, it seems worthwhile to further question the impact of the nature of the Chl field used to force the ocean model, especially for long-term simulations such as climate projections. Some studies have already addressed this issue, but not from the same angle as this study, nor in the same ocean region. For example, in Lengaigne et al. (2007), they explored the sensitivity of some oceanic physical characteristics (e.g. SST, current velocity) to this biological feedback in the Tropical Pacific Ocean, using either Chl fields derived from a biological-ocean-atmosphere coupled model or simplistic fields (constant Chl concentration values over time or space). By comparing the different simulations, they showed that the biological feedback warms the surface of the Eastern Equatorial Pacific (i.e. the upwelling and Chl-rich regions) by about 0.5 °C due to competing processes, i.e. the direct warming of the surface layer by the presence of Chl and the cooling by horizontal meridional advection of cold water. More recently, Hernandez et al. (2017) have compared simulations of the Atlantic Ocean forced by several Chl fields differing either in their surface values or in the method used to generate vertical Chl profiles (homogeneous on the vertical versus calculated by Morel and Berthon (1989)'s formulation). Their results highlighted the impact of the Chl field on surface and subsurface temperature and on upwelling systems in this region of the ocean. Finally, Berthet et al. (2023) have also shown the significant impact of the nature (model versus climatology) and the shape of profiles (homogeneous versus vertically variable) of Chl forcing on the global nitrous oxide inventory and on oxygen concentration in oxygen minimum zones. However, to the best of our knowledge, no study has been carried out to analyse in detail the effect of the nature of the forcing Chl field on the entire water column or on long-term trends in temperature profiles and vertical mixing, a fortiori in the Mediterranean Sea. Concerning the temporal frequency of the chlorophyll forcing field, in a recent study, satellite-derived Chl data with different time frequencies (monthly and monthly climatology) have been used to analyse the impact of biological feedback on oceanic and atmospheric physics when considering the interannual variation of Chl (Doi and Behera, 2022). However, their analysis was limited to the ML and spanned only a year.

The Mediterranean basin has already been identified as being particularly sensitive to climate change, and the future annual warming rate in this basin is projected to be 20% larger than the global annual average (e.g. Lionello and Scarascia, 2018). Therefore, in the present paper, we aim to investigate the long-term impact of the nature of the forcing Chl field on the vertical profile of temperature and other physical characteristics at the scale of the Mediterranean Sea. In the framework of the international Med-CORDEX inter-comparison exercise (Ruti et al., 2016), several climate projections based on RCP scenarios were produced (Soto-Navarro et al., 2020), forced by climatological and/or simplistic Chl fields. Some of these physical projections were used in a second phase to force a variety of biogeochemical models (e.g. Macias et al., 2015; Gehlen et al., 2015; Moullec et al., 2019; Pagès et al., 2020b). However, as far as we know, the impact of the forcing Chl fields on the aforementioned physical projections has not been fully investigated. The aim of the present paper is therefore (i) to characterize and quantify the consequences of using a vertically homogeneous Chl field, as commonly used in forcing ocean circulation models, on key physical features of the Mediterranean Sea, including the temperature field, stratification, and vertical mixing, (ii) to investigate the differences generated by using the same Chl field saved at three different output frequencies to force the same physical model, (iii) to put forward some potentially useful elements on the strategy to be followed to include the biological feedback of Chl in ocean circulation models for the Mediterranean Sea.

2. Material and methods

2.1. The physical model CNRM-RCSM6

In this study, the physical model refers to the fully-coupled high-resolution Regional Climate System Model CNRM-RCSM6 (http://www.umr-cnrm.fr/spip.php?article1098) dedicated to the study of the Mediterranean climate and the Mediterranean Sea. The CNRM-RCSM6 simulates the main components of the Mediterranean regional climate system and their interactions. It includes four different components, namely: (i) the atmosphere model ALADIN-v6, with interactive aerosol scheme TACTIC, with 12 km resolution and 91 levels (Nabat et al., 2020), (ii) the SURFEX v8 multisurface model (http://www.umr-cnrm.fr/surfex/spip.php?rubrique12) at the same horizontal resolution, in which each mesh is divided into four surface types: ocean, water body (lakes, etc.), urban area, natural area (soil and vegetation). Each surface type interacts with the atmosphere via a specific model, and the total flux of a mesh exchanged with the atmosphere results from the addition of the individual fluxes weighted by their respective fractions, (iii) the river routine model CTRIP (Decharme et al., 2019), with deep drainage, flood plains, and a lake parameterization (FLAKE) at a resolution of 50 km, (iv) the ocean model NEMOMED12 (Beuvier et al., 2012; Hamon et al., 2016; Waldman et al., 2018b), with a horizontal resolution of about 6 km, and 75 layers in the vertical from 1 m thickness to 134 m.

OASIS3-MCT (Craig et al., 2017) is used as the coupler, at a 1h-frequency. The modelled domain covers the Mediterranean Sea and a buffer zone (from 11 to 6°W) which includes part of the Atlantic Ocean. A relaxation to temperature, salinity and sea surface height (SSH) data from the ORAS4 reanalysis (Balmaseda et al., 2013) is performed in the buffer zone, for which the SSH seasonal cycle is corrected according to Adloff et al. (2018). Note that the rivers' runoffs are fully coupled through the CTRIP component, except for the Nile for which a climatological seasonal cycle with a yearly average of 444 $m^3.s^{-1}$ is applied (Erika Coppola, Med-CORDEX community, https://www.medcordex.eu/Med-CORDEX-2baseline-runsprotocol.pdf). This means that freshwater inputs to NEMOMED12 vary during the simulation

according to precipitation and evapo-transpiration over land. More details on CNRM-RCSM6 can be found in Voldoire et al. (2019) where it is described, and in Darmaraki et al. (2019) where it is used in the same version as the present work.

Boundary conditions for the atmospheric model are given by the ERA-interim reanalysis (Berrisford et al., 2009) with a spectral nudging (Colin et al., 2010). In the ocean model, horizontal eddy diffusion of tracers (heat, salinity) is performed along iso-neutral surfaces using a Laplacian operator, and the horizontal turbulent diffusion coefficient is set at 60 $m^2.s^1$. For momentum, diffusion is performed using a biharmonic operator with a horizontal viscosity coefficient fixed at 1.25 10^{10} $m^4.s^{-2}$. Vertical viscosity and diffusivity are obtained from a 1.5 closure scheme based on a prognostic equation for turbulent kinetic energy and a closure assumption for turbulent length scale (Blanke and Delecluse, 1993), with a vertical diffusivity coefficient that can increase up to 10 $m^2.s^{-1}$ in the case of unstable stratification. EEN (Energy and ENstrophy conserving) and TVD (Total Variation Diminishing) schemes are used respectively for momentum and tracers advection (Arakawa and Lamb, 1981; Barnier et al., 2006). Finally, a time step of 12 min is used for the numerical simulation.

2.2. The biogeochemical PFT flexible-stoichiometry model Eco3M-MED

The biogeochemical model Eco3M-MED used in this study is implemented in the modelling platform Eco3M (Baklouti et al., 2006). The Eco3M-MED model represents the planktonic web through six Plankton Functional Types (PFTs), namely meso-, micro- and nano-zooplankton, large and small phytoplankton, and heterotrophic bacteria. It has already been used and assessed by using in situ data in several studies (Alekseenko et al., 2014; Guyennon et al., 2015; Pagès et al., 2020b).

One of the main original features of this model is that each PFT is represented by a biomass expressed by several concentrations including carbon (C), nitrogen (N), phosphorous (P), and chlorophyll (Chl) concentrations, but also by an abundance (in cell or individuals per unit volume). This specificity makes it possible to calculate intracellular quotas as well as intracellular ratios, which provide valuable benefits for in-depth analysis and understanding of the functioning of the trophic web (see Baklouti et al. (2021)). Three inorganic nutrients, namely nitrate (NO_3), ammonium (NH_4), and phosphate (PO_4), as well as dissolved and particulate detrital organic material (respectively DOM and DET) are also included in the model.

Only the labile pool of DOM is explicitly represented, except for the carbon pool for which semi-labile DOC is also an explicit state variable of the model. Finally, the DET compartment is split into large and small detrital particles, associated with different sinking rates. Overall, the model includes 37 state variables. The biogeochemical processes in the model, namely photosynthesis, grazing, uptake, exudation, excretion, mineralization, chlorophyll synthesis and photoacclimatisation, mortality, respiration and nitrification, are mainly represented on a mechanistic basis, and intracellular ratios and quotas control the kinetics of most of these processes. A full description of the state variables, the equations, and the model parameters is given in Baklouti et al. (2021). The Eco3M-MED model estimates the biogeochemical sources and sinks of each biogeochemical state variable using the shortwave radiation provided by the physical model, while the transport and mixing of biogeochemical tracers is carried out in the NEMO model using the same schemes and formulations as those used for the transport/mixing of salt and heat.

2.3. Light absorption and heat budget

Incident shortwave solar radiation is absorbed by seawater in a spectrally selective manner, depending on the concentration of particles in the water. In the physical model NEMO (*cf.* Section 2.1), this absorption relies on the RGB model (Morel and Maritorena, 2001) in which visible light is divided principally into three wavelength bands: blue (400–500 nm), green (500–600 nm) and red (600–700 nm). For each wavelength band, the Chl-dependent RGB attenuation coefficient is tabulated for 61 non-uniform Chl classes ranging from 0.01 to 10 g Chl/L, and fitted to coefficients derived from a full spectral model of Morel (1988). However, it is important to note that in most ocean circulation models (including the NEMO model used in this study), all the incident shortwave irradiance absorbed by Chl is converted into heat in the water column (Madec et al., 2023), though in reality, a small part of this incoming irradiance is re-emitted through fluorescence, another part is used for photochemical reactions to produce organic matter (e.g. photosynthesis), and only the remaining portion is dissipated as heat in the seawater (Melis, 2009). Light absorption by Chl therefore impacts sea water temperature at each depth level, and the resulting temperature variation can be described by the following equation (Madec et al., 2023) :

$$\frac{\partial T(z)}{\partial t} = \frac{1}{\rho \cdot C_p} \frac{\partial I(z)}{\partial z} \quad (1)$$

In Eq. (1), z stands for depth, $T(z)$ for the temperature at depth z, C_p for the specific heat capacity of seawater, ρ for the seawater density, and $I(z)$ for the incident irradiance at depth z.

2.4. Simulations and associated forcing Chl fields used in this study

All simulations were carried out in accordance with the Med-CORDEX coupled simulation protocol (https://www.medcordex.eu/baseline-runs.php, https://www.medcordex.eu/Med-CORDEX-2_baseline-runs_protocol.pdf) and cover the period 2006–2016.

The initial physical fields are the January 01, 2006 output fields of the simulation forced by ERA-Interim over the period 1980–2018 and described in Sevault (2024). The initial biogeochemical fields are the January 2006 output fields of a similar but longer simulation which began in 1997 and which itself used as initial conditions the outputs of an earlier simulation which began in 1985. The earliest simulation is presented in Pagès et al. (2020a) and has benefited from a 20-year spin-up. The different physical simulations upon which this work is based are detailed as follows (see also Fig. 1):

1. In the SAT_VHOM simulation, the forcing Chl field is proposed by default in the NEMOMED12 model in the absence of a biogeochemical model. It is a vertically homogeneous Chl field constructed from a monthly surface Chl climatology. The latter is derived from satellite ocean colour data (L3 ESA-CCI product averaged over the period 2003–2011 as recommended by the MedCORDEX protocol, see Fig. 2). Since satellite-derived Chl data only provide 2D fields (i.e. surface Chl concentrations), the vertically homogeneous 3D field was constructed by assigning the surface Chl concentration value to the entire water column. In other words, the Chl concentration remains equal to the surface value throughout the water column.
2. The other three Chl fields originate from the same 3D Chl field that was calculated by the Eco3M-MED model (Baklouti et al., 2021) forced offline by the NEMOMED12 physical model, but saved at three different frequencies, i.e. monthly climatological, monthly, and daily (see Fig. 1). These three Chl fields were used in turn to force the NEMOMED12 physical model in the three simulations designated as MOD_CLIM, MOD_MONTH, and MOD_DAY, respectively.
3. Finally, the last Chl field has been generated in an original way, combining satellite and modelling data. It is made up of the same 2D satellite Chl data used in SAT_VHOM for the surface grid meshes, but reproduces the vertical shape of the Chl field calculated by Eco3M-MED below the surface. To this end, a dimensionless vertical distribution was constructed from the MOD_CLIM simulation, by dividing the modelled Chl concentrations in each grid cell within the water column by the

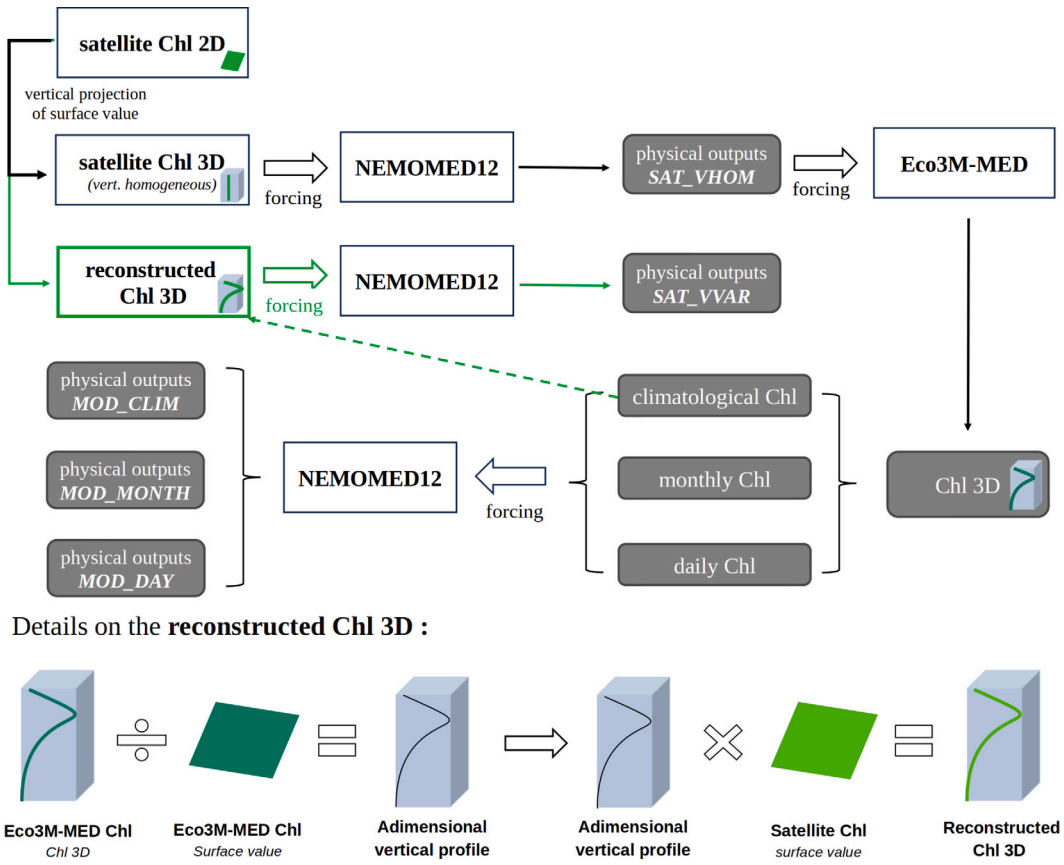

Fig. 1. Articulation of the different physical simulations in this study, differing only in the Chl field used to force them. Physical outputs include sea water temperature, salinity, density, current velocity, sea surface height, and mixed layer depth. Note that in the physical model used in this study, the NEMOMED12 model is embedded in the CNRM-RCSM6 platform (*cf.* Section 2.1).

corresponding surface Chl concentration. This dimensionless Chl field was then multiplied by the surface Chl values provided by the 2D satellite climatology (see also Fig. 1). The simulation using the latter field to force the NEMOMED12 model is called SAT_VVAR.

2.5. Diagnostics

The results and the associated discussion are partly based on the Mixed Layer Depth (MLD) and the Stratification Index (SI). The MLD is calculated in real-time by the NEMOMED12 model, and determined using a turbocline criterion, namely $K_z = 5.10^{-4}\,\mathrm{m^2 s^{-1}}$ as a threshold for the bottom of the mixed layer (Somot et al., 2018; Madec et al., 2023).

The SI quantifies the vertical stratification in a water column from the surface to a selected depth H (sea bottom in this study). Here, the formulation for SI is given by Somot (2005):

$$SI = \int_0^H N^2(z) \cdot z \, dz \tag{2}$$

In Eq. (2), z is the vertical depth, and N represents the Brunt–Vaisala frequency.

In this study, we will focus on three diagnostics, namely the monthly-averaged MLD (MLD-mean), the maximum daily MLD within one month (MLD-max), and the evolution of monthly variations in SI.

2.6. Study region

The Mediterranean Sea (MED) is a semi-enclosed sea encompassing two basins, i.e. the Western Mediterranean (MEDW) and the Eastern Mediterranean (MEDE), linked by the Strait of Sicily. Its average depth is 1500 m and the deepest point is 5109 m in the Ionian Sea. There is a wealth of literature describing its circulation and main characteristics (e.g. Millot and Taupier-Letage, 2005; Durrieu de Madron et al., 2011; Waldman et al., 2018a) and only a few elements are given here. The MED circulation is characterized by three predominant interacting spatial scales: the basin-scale circulation composed of surface flow of water from the Atlantic and a return flow of intermediate water originating from the Levantine Basin. On sub-basin scale, cyclonic gyres are present in the MEDW and MEDE, mainly driven by thermohaline circulation (Malanotte-Rizzoli et al., 2014). Finally, the MED Sea is characterized by an intense (sub)mesoscale activity (e.g. Bosse et al., 2016; Mason et al., 2023). The MED Sea has long been considered an interesting miniature laboratory for oceanographic research (Malanotte-Rizzoli et al., 1999), due to the similarity between the processes and forcings active there and those of the global ocean. Predicting the impact of rapid climate change in the Mediterranean is therefore essential for a better understanding of changes on a global scale. Due to the spatial variability of Chl concentration (Fig. 2), this study focuses not only on the entire MED but on three sub-basins (Fig. 3). The mixed layer depth (MLD), a key physical characteristic for biogeochemistry, varies significantly across these sub-basins. In the MEDW, and especially in the NorthWestern Mediterranean (MEDNW), convection processes and deep water formation are observed in winter, and the MLD can reach the seabed (2500 m) in MEDNW (Waldman et al., 2016; Courtois et al., 2017). As a consequence, a marked spring bloom can be observed in this region (Fig. 2). Conversely, in the MEDE, Levantine Intermediate Water (LIW) is produced in winter in the Levantine Basin and circulates between 300 and 500 m deep towards the Strait of Sicily (Robinson et al., 1991; Pinardi et al., 2002). The

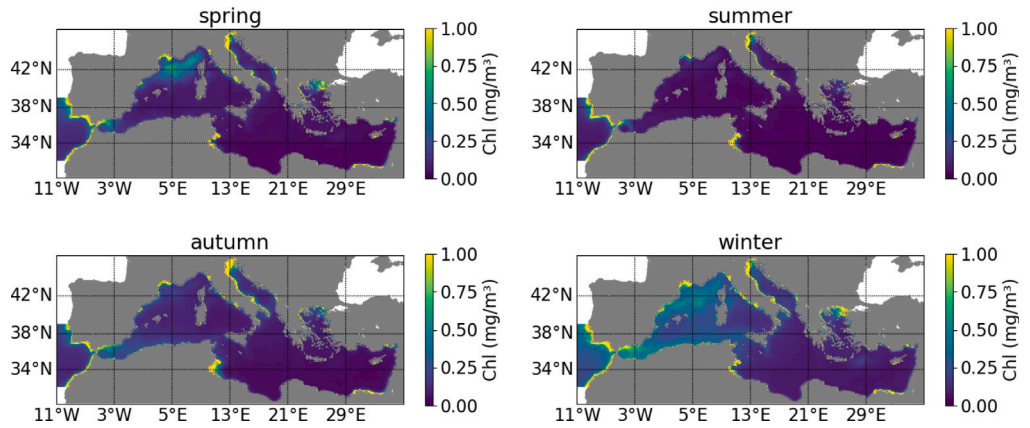

Fig. 2. Seasonal climatology of surface Chl concentrations derived from the ocean colour satellite data (ESA-CCI L3 dataset) for the period 2003–2011.

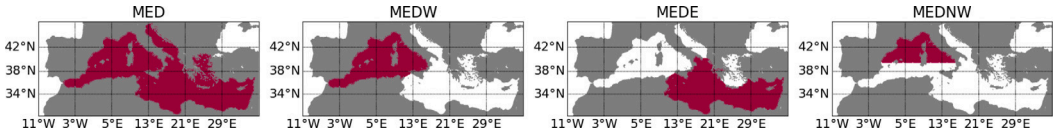

Fig. 3. The sub-basins of the Mediterranean Sea considered in this study: Entire Mediterranean (MED), Western Mediterranean (MEDW), Eastern Mediterranean (MEDE), and Northwestern Mediterranean (MEDNW).

maximum MLD in MEDE is shallower than in MEDW and the Chl content is lower than in MEDW due to ultra-oligotrophic conditions. Finally, the study distinguishes three layers in the water column: the surface layer (SL, 0–150 m), sometimes divided in this work into the upper surface layer (USL, 0–70 m) and the lower surface layer (LSL, 70–150 m) for analysis purposes, the intermediate layer (IL, 150–600 m) and the bottom layer (BL, > 600 m). These three layers correspond respectively to the productive layer, the layer including LIW waters, and the bottom layer, which is rarely influenced by vertical convection.

2.7. Statistical/Mathematical tools

The statistical and mathematical tools used in this work are described as follows:

- **Characterization of the trend: identification, significance**
  The Mann–Kendall statistical test (Mann, 1945; Stuart, 1956) is a non-parametric technique, widely used to detect trends in time series. This test considers two hypotheses: H_0 (accepted): there is no trend in the time series (*p-value* > 0.05) and H_a (rejected): a trend is present in the time series (*p-value* < 0.05). Using this statistical test, we can determine whether or not a trend exists in a time series. Furthermore, for identifying potential trends in time series characterized by seasonal variability, the Seasonal Kendall test, a specific version of the Mann–Kendall (MK) test, is commonly used (Hirsch et al., 1982). In this study, after confirming the significance of a trend through the MK test, we estimate the associated slope using Sen's method (Sen, 1968). Sen's method computes the slope as the median of all slopes calculated between each pair of points in the time series.
- **The ΔT_{10} concept**
  As we will see in the Results section, the trend in temperature difference between two given simulations will generally consist of very low values that are difficult to interpret. We will therefore use instead the concept of ΔT_{10}, which is the temperature difference generated after 10 years if the trend remained the same. This is a much more concrete (and meaningful) quantity, since it is a temperature difference, and its order of magnitude is easier to interpret. Note that ΔT_{10} can also be interpreted as a trend expressed in decades, which is why we will also consider ΔT_{10} as a trend in the text.
- **Trend elimination**
  To eliminate polynomial trends from the time series produced by the model, we used the first-order differentiation method which calculates the detrended signal by the following formula (Canova, 1998):

$$\widetilde{X_t} = \nabla X_t = X_t - X_{t-1} \tag{3}$$

  In Eq. (3), $\widetilde{X_t}$ represents the detrended signal at time t, and X_t, X_{t-1} represent consecutive data in the time series.
- **Coefficient of correlation**
  The correlation coefficient quantifies the degree of correlation between two variables (Pearson, 1909). The formula for calculating the correlation coefficient (r), here for two times series X and Y, is given by:

$$r = \frac{cov(X,Y)}{\sigma_X \sigma_Y} \tag{4}$$

  In Eq. (4), $cov(X,Y)$ stands for the covariance of X and Y, and σ_X and σ_Y represent the standard deviation of X, Y. The absolute value of r is within the range of 0 to 1, with values closer to 1 indicating a stronger correlation between variables.

2.8. Differences between simulations

For a given 3D variable such as temperature, the difference between the space averaged temperatures provided by two simulations (sim and ref) over the region reg (see Fig. 3) and the layer lay (lay is either the surface (0–150 m), the intermediate (150–600 m), or the bottom (600 m-bottom) layer, or the whole water column), is given by:

$$\Delta T^{reg}_{lay} = \left(\sum_{i,j \in reg} \sum_{k \in lay} T^{sim}_{ijk} \times V_{ijk} \right) / V^{reg}_{lay} - \left(\sum_{i,j \in reg} \sum_{k \in lay} T^{ref}_{ijk} \times V_{ijk} \right) / V^{reg}_{lay} \tag{5}$$

where i, j, k are the grid mesh indices in the longitudinal, latitudinal, and vertical directions respectively, and V_{ijk} is the volume of this mesh. V^{reg}_{lay} is the volume of water of the region reg over the layer lay. ΔT^{reg}_{lay} as defined in this equation is then a function of time. For 2D variables such as SI and MLD, the difference between their values provided by two

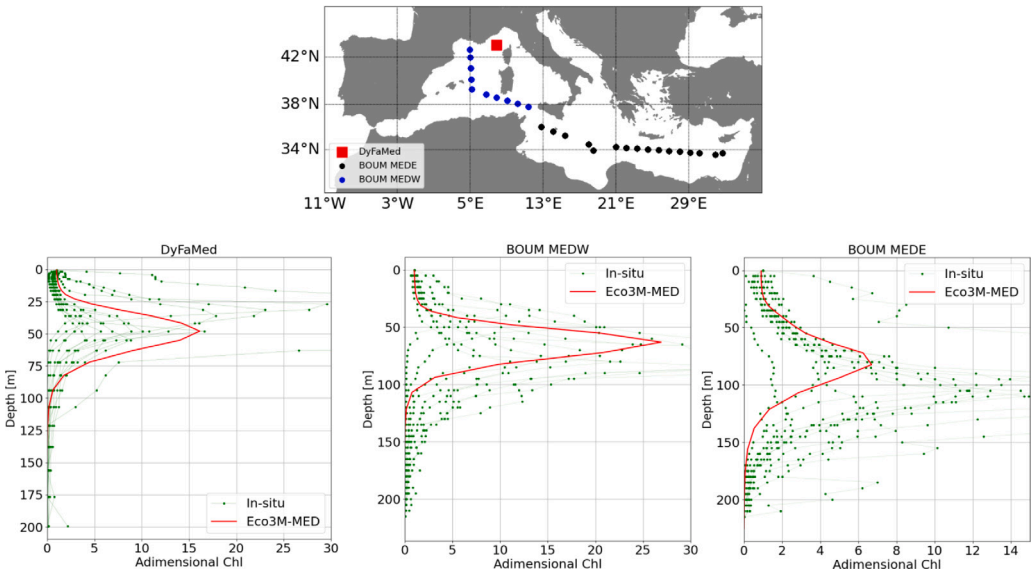

Fig. 4. Comparison of modelled and measured adimensional (i.e. normalized by the surface value) summer Chl concentrations. The modelled Chl is provided by the Eco3M-MED model forced by NEMOMED12 (i.e. it is a Chl climatology derived from simulation MOD_CLIM) and in situ data are from DyFaMed site and BOUM cruise section (Moutin et al., 2012). The DyFaMed data (Coppola et al., 2023) can be accessed via the URL: https://www.seanoe.org/data/00326/43749/ and BOUM data were extracted from the open source PERSEUS database (https://isramar.ocean.org.il/PERSEUS_Data).

simulations sim and ref over the region, reg is given by (for example for SI):

$$\Delta \mathrm{SI}^{reg} = \left(\sum_{i,j \in reg} \mathrm{SI}_{ij}^{sim} \right) / n_{reg} - \left(\sum_{i,j \in reg} \mathrm{SI}_{ij}^{ref} \right) / n_{reg} \quad (6)$$

where n_{reg} is the number of grid meshes in region reg. $\Delta \mathrm{SI}^{reg}$ as defined in this equation is also a function of time.

The differences in MLD-max is calculated as follows:

$$\Delta \text{MLD-max}^{reg} = \left(\max_{i,j \in reg} \mathrm{MLD}_{ij}^{sim} \right) - \left(\max_{i,j \in reg} \mathrm{MLD}_{ij}^{ref} \right) \quad (7)$$

The difference in the vertically integrated Chl is expressed as follows:

$$\Delta \mathrm{Chl}_{lay}^{reg} = \left(\sum_{i,j \in reg} \sum_{k \in lay} \mathrm{Chl}_{ijk}^{sim} \times V_{ijk} \right) - \left(\sum_{i,j \in reg} \sum_{k \in lay} \mathrm{Chl}_{ijk}^{ref} \times V_{ijk} \right) \quad (8)$$

Finally, it is important to note that for the comparison between the two simulations forced by Chl fields differing only in their vertical aspect (i.e. the simulations SAT_VHOM where Chl is vertically-homogeneous and SAT_VVAR for which the vertical variability is provided by the Eco3M-Med model, cf. Section 2.4), we will base our analysis on the difference between SAT_VHOM and SAT_VVAR (i.e. SAT_VHOM - SAT_VVAR), whereas for the comparisons of the MOD_CLIM, MOD_MONTH, and MOD_DAY simulations, the reference is MOD_DAY and all differences will be calculated relative to MOD_DAY.

3. Model skill assessment with in situ data

The Eco3M-MED model has already been quite extensively compared with in situ data (Guyennon et al., 2015; Pagès et al., 2020a; Baklouti et al., 2021), illustrating its capacity to reproduce the key features of the biogeochemistry of the Mediterranean Sea. Here, we provide additional comparisons focused on the vertical profiles of Chl (Fig. 4). A further comparison with Chl data is also available in Fig. SM5.

With the above results we consider that the vertical variability of the Chl field is quite well represented by the Eco3M-MED model, and in any case the model allows a better representation of the vertical profiles of Chl than a vertically homogeneous profile.

Table 1
Relative difference (in percent) on the quantity of Chl read by the model accumulated over one year between SAT_VHOM and SAT_VVAR (i.e., $(\mathrm{Chl}_{\mathrm{SAT\_VHOM}} - \mathrm{Chl}_{\mathrm{SAT\_VVAR}})/\mathrm{Chl}_{\mathrm{SAT\_VHOM}}$).

Layer	MED	MEDW	MEDE	MEDNW
ΔChl 0–70 m	−66.2%	−96.1%	−37.0%	−89.2%
ΔChl 70–150 m	36.4%	39.0%	26.1%	45.0%
ΔChl 150–600 m	98.8%	99.3%	98.5%	98.8%

4. Results

4.1. Effect of the vertical variability of Chl: comparison of SAT_VHOM and SAT_VVAR simulations

4.1.1. Quantitative differences between Chl forcing fields

The difference in Chl quantity in each layer between the SAT_VHOM and SAT_VVAR Chl fields is summarized in Table 1. It can be seen that in the upper surface layer (0–70 m), the amount of Chl is higher in the SAT_VVAR forcing field than in SAT_VHOM one, especially in the Western Mediterranean, due to the presence of a DCM (Deep Chlorophyll Maximum) in SAT_VVAR which is not present in SAT_VHOM. Moreover, since the DCM is deeper and less intense in MEDE, the excess of Chl in SAT_VVAR is lower in MEDE than in MEDW between 0 and 70 m. Below 70 m, the amount of Chl is always higher in SAT_VHOM, especially below 150 m where there is almost no more Chl in the model-derived climatology, whereas there is always as much as at the surface in the satellite climatology.

The difference in the mean Chl profile over the MED between the SAT_VVAR and SAT_VHOM simulations is shown in Fig. 5 for two contrasting seasons. In winter, the excess of Chl in SAT_VHOM compared with SAT_VVAR increases with depth. By contrast, the Chl concentration in summer is higher in SAT_VVAR from about 20 m down to 120 m, due to the presence of a DCM in SAT_VVAR that is not present in SAT_VHOM.

4.1.2. Decadal trend in the difference between SAT_VHOM and SAT_VVAR

The difference (ΔT) in averaged temperatures over the Mediterranean basin between the two simulations (see Eq. (5)) is shown in Fig. 6 as a function of time. This difference is also shown for the

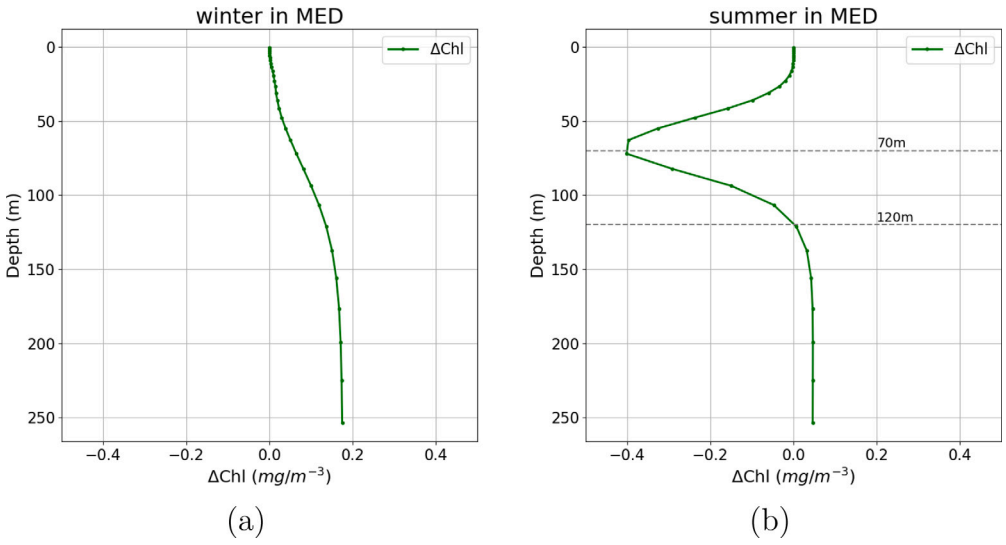

Fig. 5. Mean ΔChl between SAT_VHOM and SAT_VVAR over the Mediterranean Sea (a) in winter and (b) in summer.

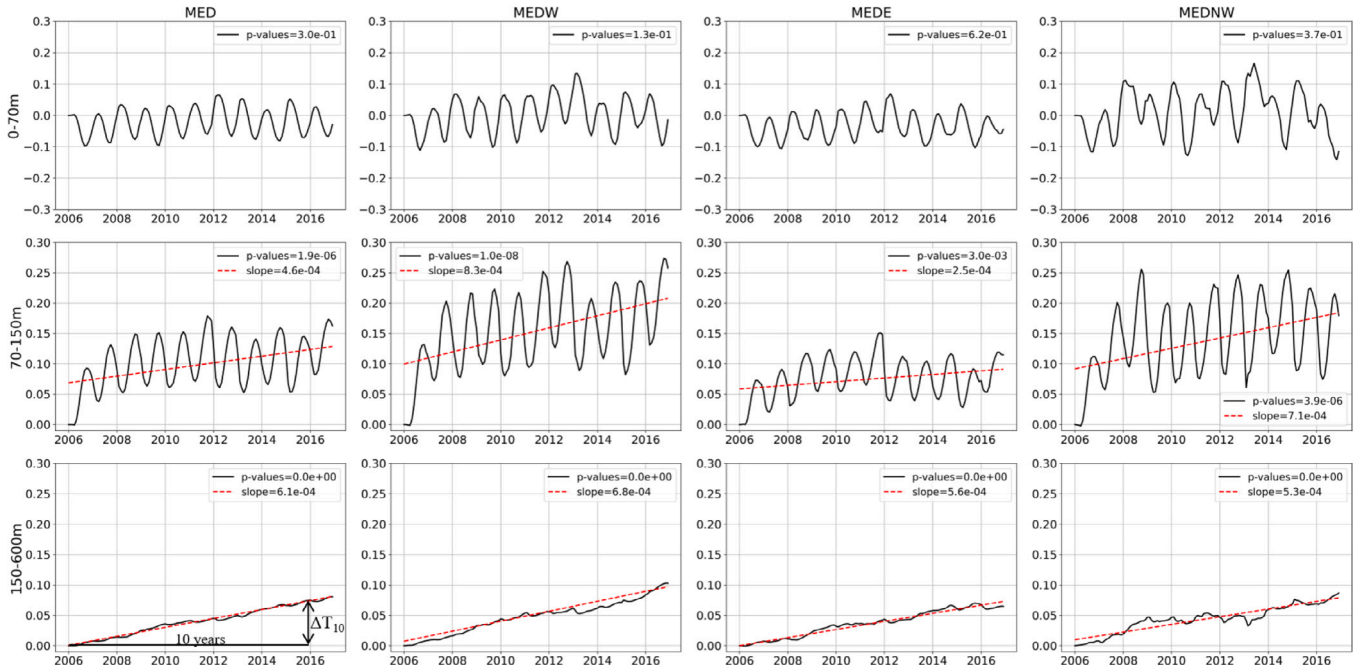

Fig. 6. Difference (ΔT) between SAT_VHOM and SAT_VVAR (i.e. T(SAT_VHOM) - T(SAT_VVAR)) in the temperature averaged over different layers and basins as defined in Section 2.6. The black line shows the raw data series and the dotted, red line represents the trend calculated using Sen's method after the MK test has confirmed its significance. The ΔT_{10} concept is described in Section 2.7 and illustrated in the figure at the bottom left.

different layers and sub-regions previously defined (*cf.* Section 2.6). It can be seen that the sign of ΔT varies in the upper surface layer while it remains positive below the USL. Moreover, in the entire basin, as well as within each region and layer, $|\Delta T|$ exhibits an increasing trend over time. To assess the statistical significance of the corresponding trends, the Mann–Kendall test (*cf.* Section 2.7) was applied.

Except in the upper surface layer, all the trends turned out to be significant in the temperature difference (ΔT) (Fig. 6). For simplicity, in the remaining of this paper, trends will be represented by the temperature difference generated after 10 years (noted ΔT_{10}) between the SAT_VHOM and SAT_VVAR simulations (see Section 2.7 for the definition of ΔT_{10}).

Table 2
Trend in the temperature difference between SAT_VHOM and SAT_VVAR for each sub-basin and layer calculated by the Sen's method (see Section 2.7). For the sake of simplicity, trends are represented by ΔT_{10} values (cf. Section 2.7 and Fig. 6). The "/" in the table indicates that there is no trend in the layer.

Layer	MED	MEDW	MEDE	MEDNW
ΔT_{10} 0–70 m	/	/	/	/
ΔT_{10} 70–150 m	0.05 °C	0.1 °C	0.03 °C	0.08 °C
ΔT_{10} 150–600 m	0.07 °C	0.08 °C	0.07 °C	0.06 °C
ΔT_{10} 600m-BOT	−0.0003 °C	0.001 °C	−0.002 °C	0.004 °C

It can also be seen that ΔT_{10} is positive almost everywhere (Table 2), which indicates that SAT_VHOM is warmer than SAT_VVAR.

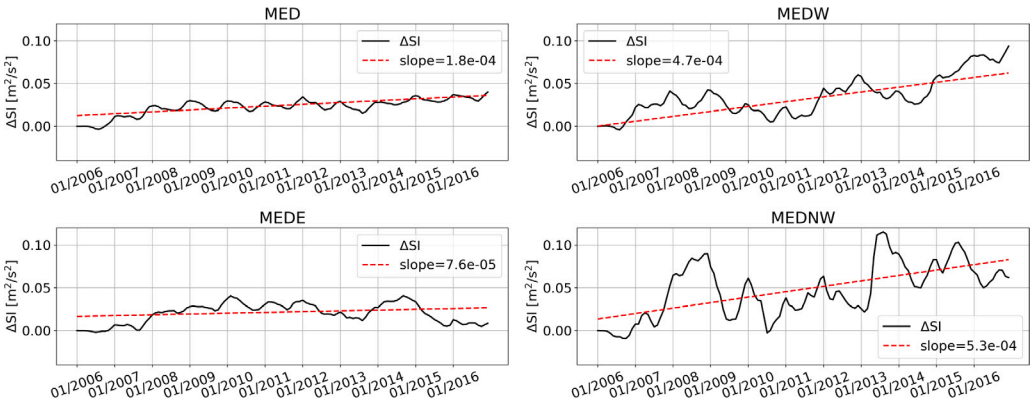

Fig. 7. Stratification index difference (ΔSI) between SAT_VHOM and SAT_VVAR in different basins. The black line shows the raw series and the dotted red line represents the trend calculated using Sen's method.

The highest trends are in the lower surface layer (up to 0.1 °C) in the MEDW sub-basin, and in the intermediate layer (<0.07 °C) in the MEDE sub-basin. We can also notice that $|\Delta T_{10}|$ values are globally lower in the MEDE than in MEDW sub-basin and that they are very low in the bottom layer.

Similarly, the difference (ΔSI) between the average stratification indices (*cf.* Section 2.5) has been calculated for the different sub-basins (Fig. 7), showing a positive trend over time, with the highest trends in the western sub-basin, and especially in the MEDNW.

In contrast, no trend was observed for the mixed layer depth difference (ΔMLD), which exhibits only interannual variability (See Fig. SM1 in the Supplementary Material).

4.1.3. Seasonal and vertical variability of the difference between SAT_VHOM and SAT_VVAR

The evolution over time and depth of ΔT (Fig. 8) exhibits marked seasonal variations associated with vertical variability in the surface layer. Note that the mean MLD values of the two simulations are superimposed on this figure, and that the same figure on which the maximum MLD values are superimposed is available in the Supplementary Material (Fig. SM2) . In 2006, after the winter mixing during which ΔT is close to zero in the surface layer, this layer progressively splits into an upper layer (above ≈ 70 m) where ΔT is negative and a lower layer (between 70 and 150 m) where ΔT is positive until the next winter reducing the temperature difference to a value close to zero. This cycle repeats itself almost identically every year in the MED and all its sub-basins (Figs. 8a and b), except that the reduction in ΔT with winter mixing is less and less pronounced over time.

In the intermediate layer, seasonal variations are much less pronounced, and ΔT is either positive in the upper part of this layer or zero. Over the years, the region where ΔT is positive extends deeper and deeper into the intermediate layer.

A synthetic view of the seasonal variations of ΔT in the upper surface layer (Fig. 9(a)) shows that overall, ΔT 0–70m increases with ΔChl 0–70 m (i.e. roughly during winter and spring), and decreases with ΔChl0–70 m the rest of the year. The correlation coefficient *r* between these two signals from which the trend has been removed is 0.53.

In the lower surface and intermediate layers (Fig. 9(b) and (c)), the opposite occurs, namely, ΔT increases when ΔChl 0–70 m decreases, and decreases when ΔChl 0–70 m increases, which is more obvious to observe on the detrended temperature difference (see Section 2.7 for the derivation of the detrended signals). The correlation coefficient between $\widetilde{\Delta T}$ 70–600 m and ΔChl 0–70 m is −0.83. Note that it is the upper surface value of ΔChl that is used for the analysis of correlations over the entire water column since it corresponds to the layer where Chl concentrations are highest. However, the variation in $\widetilde{\Delta T}$ 600m-bottom shows no correlation with ΔChl 0–70 m (r=0.02), nor is there a clear correlation between ΔMLD-max and $\widetilde{\Delta T}$ 70–600 m (r=0.26).

Table 3
Mean difference in temperature (in °C) between MOD_CLIM and MOD_DAY, and MOD_MONTH and MOD_DAY, in the surface (SL), intermediate (IL) and bottom (BL) layers over the simulated 11 years in MED. Mean ΔT ($|\Delta T|$) values are determined from ΔT ($|\Delta T|$) values averaged over time and space on each layer (see Section 2.8) .

Layers	MOD_CLIM - MOD_DAY		MOD_MONTH - MOD_DAY	
	Mean ΔT	Mean $\lvert\Delta T\rvert$	Mean ΔT	Mean $\lvert\Delta T\rvert$
SL	−0.0074	0.018	−0.0063	0.012
IL	−0.0079	0.010	−0.0020	0.007
BL	0.0021	0.003	0.0013	0.003

4.2. Impact of the temporal frequency of the Chl fields

In this section, we present the results of the comparison between the simulations MOD_CLIM, MOD_MONTH, and MOD_DAY (i.e. MOD_CLIM - MOD_DAY and MOD_MONTH - MOD_DAY). The mean of ΔT and $|\Delta T|$ values between simulations are summarized in Table 3 for each layer, showing first that all these differences are very weak. However, the temperature differences between MOD_CLIM and MOD_DAY are greater than those between MOD_MONTH and MOD_DAY. It can also be noticed that the mean ΔT is negative (i.e. MOD_DAY is on average warmer than the two other simulations) in the surface and intermediate layers and that it is positive in the bottom layer (Table 3 and Figure SM3 in the Supplementary Material).

The presence of trends in the difference between simulations was analysed using the Mann–Kendall test, showing the presence of trends in the temporal evolution of ΔT (Fig. 10) and ΔSI (not shown), while those of ΔMLD and ΔChl 0–150 m showed no significant trends.

Furthermore, when temperature difference trends are significant, they are of the same sign (i.e. negative here) within the surface and intermediate layers, and of the opposite sign (i.e. positive) in the deep layer. In all the basins where the trend (i.e. ΔT_{10}) is significant, the highest values of this trend are found in the surface layer when comparing MOD_MONTH and MOD_DAY, but in the intermediate layer when comparing MOD_CLIM and MOD_DAY (Fig. 10). Additionally, the maximum absolute value of ΔT_{10} is approximately 0.03 °C, obtained in the IL of the MEDW basin when comparing MOD_CLIM and MOD_DAY.

5. Discussion

5.1. Vertical variability of Chl has a major impact on temperature profiles

5.1.1. Preliminary analysis of the effect of Chl forcing

Though the SAT_VHOM and SAT_VVAR simulations (and all the simulations this work is based on) are the product of a two-way coupled ocean–atmospheric model, we can consider to first order that the incident shortwave irradiance is the same for all the simulations

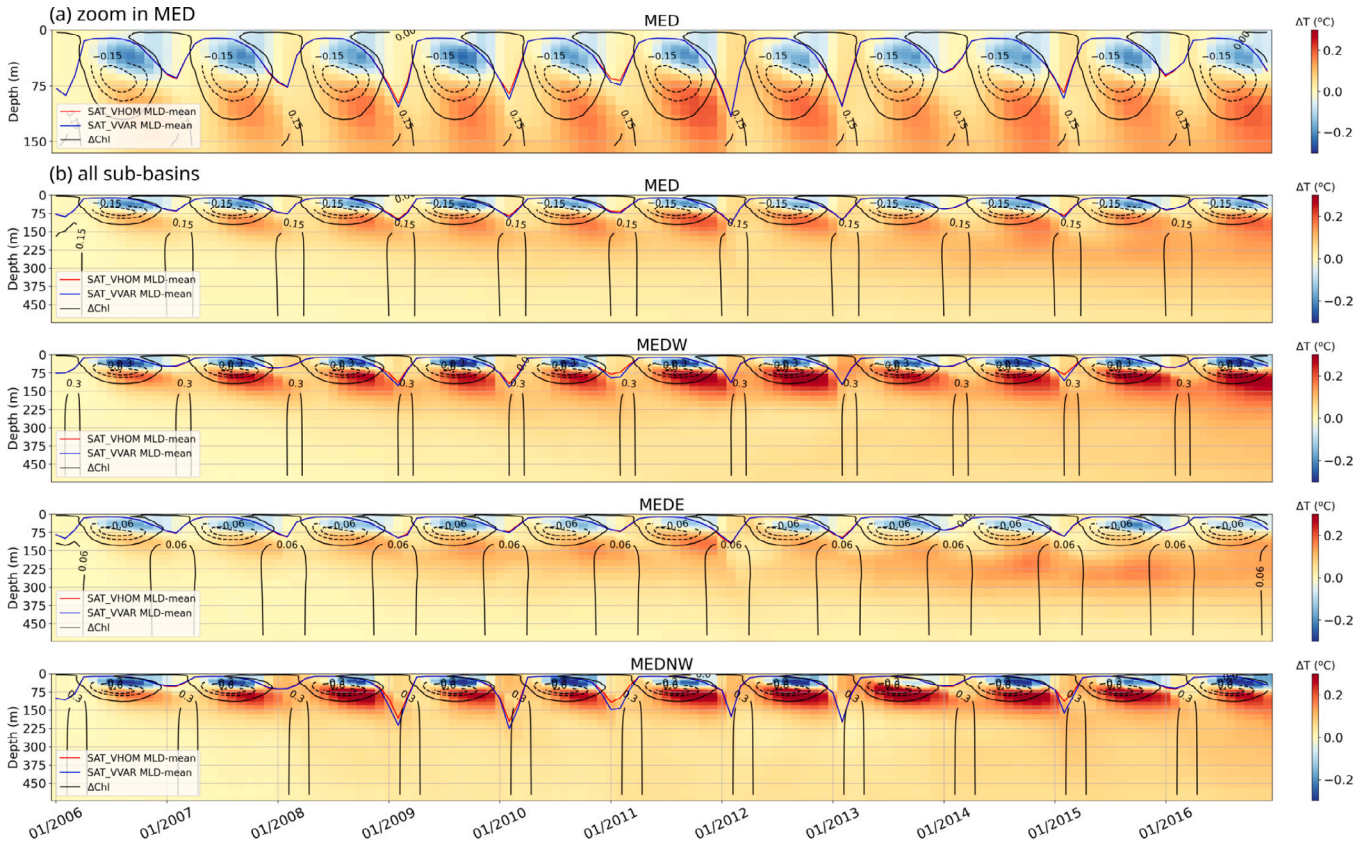

Fig. 8. Time-depth evolution of ΔT between the SAT_VHOM and SAT_VVAR simulations. The black contours indicate the iso-lines of the Chl concentration difference (unit: mg/m^3), the dashed contour represents the position of the DCM represented in SAT_VVAR, and the red and blue lines represent the monthly averaged MLD of SAT_VHOM and SAT_VVAR, respectively. (a) zoom on the surface layer (0–150 m) for the entire MED, (b) MED, and sub-basins between 0 and 450 m.

(differences lower than 0.1% were calculated, results not shown). Based on these considerations, we can assume that the energy entering the ocean via solar shortwave radiation is the same for all the simulations used in this paper. Similarly, the difference between the net air-sea fluxes of the two simulations is very small (< 4%) and shows no trend. Consequently, in the remainder of the paper, we consider that the differences in the temperature field between SAT_VHOM and SAT_VVAR are solely attributable to the direct effect of the difference in the forcing Chl field, since the indirect effect of using different forcing Chl fields via shortwave radiation and air-sea fluxes can be neglected to first order.

In addition, in the NEMO physical model, all the absorbed radiation by Chl (and water) is transformed into heat (*cf.* Section 2.3). Hence, since the Chl content is higher in SAT_VHOM than in SAT_VVAR, except in the upper surface layer (see the cumulative annual Chl in Table 1), we can expect the temperature difference (ΔT) between SAT_VHOM and SAT_VVAR to be negative and positive within and under the upper surface layer, respectively (*cf.* Fig. 6). This simplistic view is, however, modulated by seasonal and interannual variations.

5.1.2. Winter mixing does not prevent heat accumulation in the lower surface layer in SAT_VHOM

Due to seasonal variations in physical forcing and because ΔChl varies not only with season but also with depth, the temperature difference (ΔT) between SAT_VHOM and SAT_VVAR also varies with season, particularly in the surface layer, and with depth (Figs. 6 and 8). During winter mixing, Chl concentrations are low in both simulations and fairly homogeneous (although decreasing slightly) over the vertical in SAT_VVAR. As a result, $|\Delta$Chl 0–70m$|$ and $|\Delta T$ 0–70 m$|$ values are small (Fig. 9). Just after the spring bloom ΔChl 0–70 m values start to decrease and become negative with the onset of a DCM (reaching 70–80 m in summer) in SAT_VVAR.

Since from the onset of a DCM, Chl is in excess in SAT_VVAR over almost the entire SL (i.e. roughly between 0 and 120 m, see Fig. 5), more of the incident irradiance is absorbed at these depths in SAT_VVAR than in SAT_VHOM, and this excess heat in SAT_VVAR results in negative ΔT values, but only down to around 70 m (i.e. to the depth of the DCM peak). Below 70 m, ΔT values become positive due to a competing effect that becomes dominant: since more of the incident radiation has been absorbed by Chl between 0 and 70 m in SAT_VVAR than in SAT_VHOM, the residual radiation is higher in the surface layer in SAT_VHOM, leading to greater potential absorption of solar radiation by water and Chl in SAT_VHOM. Below 70 m, this effect becomes strong enough for the temperature to become higher in SAT_VHOM, even though the Chl concentration is still lower than in SAT_VVAR, down to around 120 m (see Fig. 5). Another consequence of this competing effect is that light can penetrate deeper in SAT_VHOM and be absorbed by Chl in deeper layers. Under 120 m, Chl concentrations are higher in SAT_VHOM, resulting in an ever-present (although less intense) excess heat in SAT_VHOM (i.e. a positive ΔT) to around 180 m, namely below the bottom of the surface layer (Fig. 8(b)).

The absence of DCM in SAT_VHOM is therefore responsible for the heat deficit in the upper surface layer compared with SAT_VVAR, and for the heat excess below the DCM peak (i.e. below around 70 m in this simulation). Furthermore, these heat deficit and excess in SAT_VHOM do not fully compensate for each other. Thus, while the deficit in the upper SL will be almost erased by winter mixing thanks to the heat taken from the excess heat located deeper by the deepening of the MLD, most of the heat accumulated below the mean MLD, i.e. $\approx$ 70 m, will remain there, thus intensifying each winter the excess heat in SAT_VHOM in the lower SL and the upper intermediate layer.

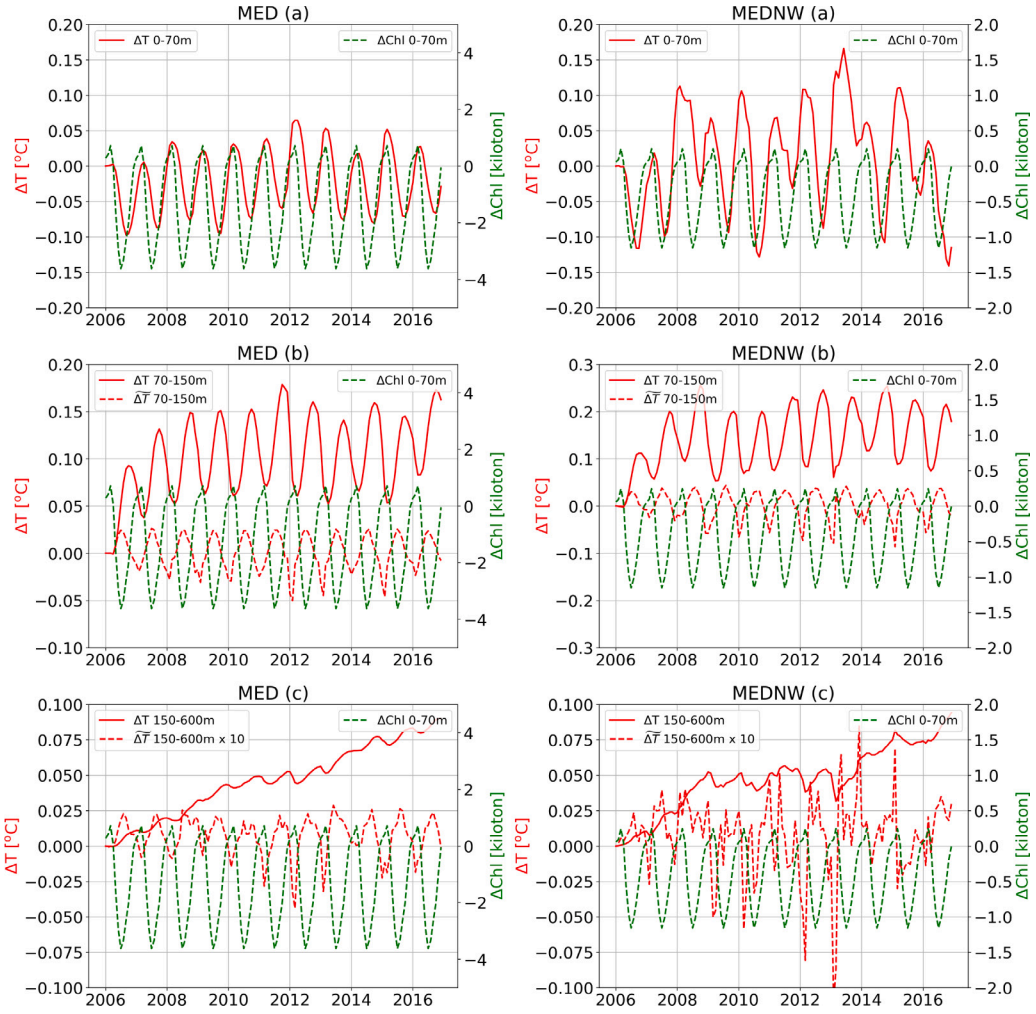

Fig. 9. Temperature difference with and without trend (ΔT and $\widetilde{\Delta T}$, respectively) and Chl 0–70 m difference (ΔChl 0–70 m) between SAT_VHOM and SAT_VVAR simulations (i.e. SAT_VHOM - SAT_VVAR) in MED. The red line represents the variation in ΔT in the (a) upper surface layer (USL), (b) lower surface layer (LSL), and (c) intermediate layer (IL), and the dotted green line shows the seasonal cycle of ΔChl 0–70 m.

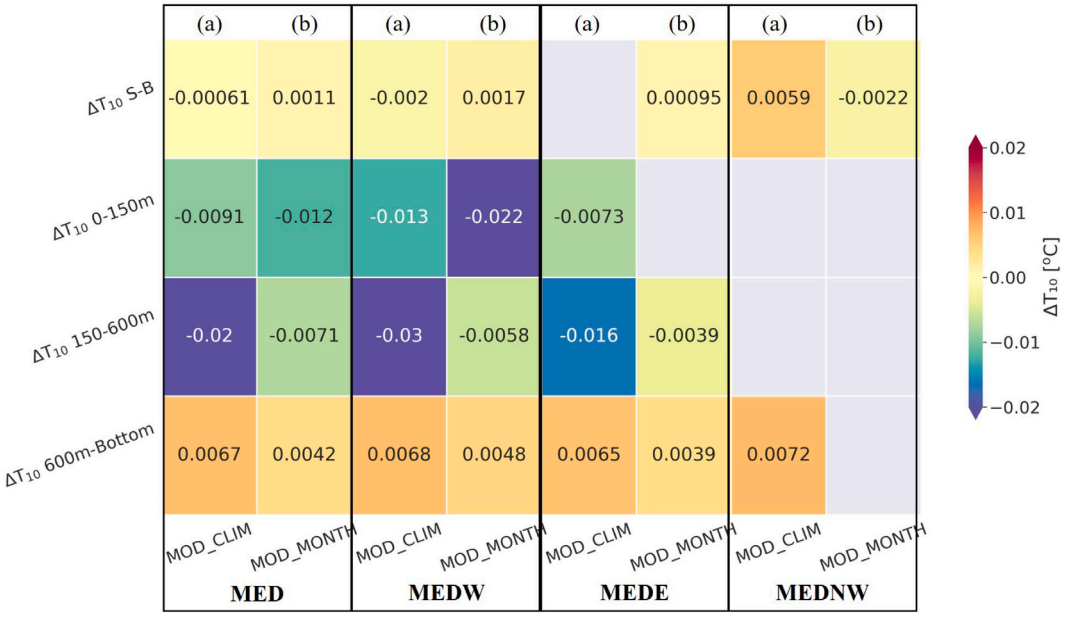

Fig. 10. Trend (represented through ΔT_{10}, see Fig. 6, and calculated by the Sen's method) in temperature difference between (a) simulations MOD_CLIM and MOD_DAY and (b) between MOD_MONTH and MOD_DAY. The coloured bar represents the scale of ΔT_{10} values, and the grey boxes indicate cases where the trend could not be determined.

5.1.3. A significant bias in SAT_VHOM on the temperature in the lower surface and intermediate layers

As mentioned before, heat excess and accumulation in SAT_VHOM (as compared to SAT_VVAR) in the lower surface and intermediate layers takes place from late spring to autumn, when the DCM is present (see Fig. 9). During winter, the heat excess in these layers decreases, but winter mixing is on average not deep or intense enough (see the mean and maximum MLD respectively in Figs. 8 and SM2) to remove all the heat previously accumulated, and ΔT remains positive (Fig. 9). Even in MEDNW where winter convection can be intense and deep, heat accumulation occurs in SAT_VHOM (Fig. 9).

In addition, the excess heat spreads downward by vertical mixing, especially during winter, resulting in a gradual thickening of the area affected by the excess heat, well below 200 m (Fig. 8), which is in line with the conclusions of Skákala et al. (2022) regarding the depth of biological feedback. The increase over time of the excess heat in SAT_VHOM will therefore create a positive trend in the temperature difference between SAT_VHOM and SAT_VVAR in the intermediate layer (150–600 m). This trend is of the same order of magnitude as the one in the LSL in MEDW, but significantly higher than that in the LSL in MEDE (Fig. 6 and Table 2). The trend of heat accumulation in SAT_VHOM is indeed nearly twice as high in the intermediate layer as in the lower surface layer in MEDE. This can be explained by the depth of the DCM which is greater in MEDE than in MEDW, inducing excess heat which is localized deeper in MEDE, combined with shallower winter mixing than in MEDW which prevents the extraction of the excess heat accumulated below 150 m.

Finally, though winter mixing is generally deeper and more intense in the MEDW than in the MEDE, the highest trend of heat accumulation is found in the MEDW since Chl concentrations are higher in the oligotrophic MEDW than in the ultra-oligotrophic MEDE (Siokou Frangou et al., 2010).

Overall, the excess heat in the intermediate layer due to the use of a homogeneous vertical profile of Chl results in a bias in temperature increasing with time. After 100 years (i.e. the typical duration of climate projections), if the determined trend were to remain the same, this bias could be as high as 1 °C in the lower surface layer in MEDW and 0.8 °C in the intermediate layer, which is far from negligible.

5.1.4. Consequences of using a vertically homogeneous Chl profile on the bottom layer

By contrast, the absolute value of the 10-year trend $|\Delta T_{10}|$ is very small (but significant) in the bottom layer (> 600 m). These lower values are partly explained by the fact that, since the water volume in this layer is much higher than the upper layers, the impact of a heat deficit/excess is much more diluted and less visible on temperature. Furthermore, these weak trends can also be explained by the compensation of two processes acting in opposite ways on ΔT, namely turbulent mixing, which brings from near to near some of the excess heat into the BL, but also convection of the heat deficit from the upper surface layer towards the bottom.

Finally, since SAT_VHOM is colder (except in winter) than SAT_VVAR only in the upper surface layer but warmer everywhere else in the water column, the integrated stratification index over the water column is higher in SAT_VHOM and the difference in stratification index increases over time, mainly in the MEDW (Fig. 7). Despite this excess stratification in SAT_VHOM compared to SAT_VVAR, there is no trend in ΔMLD, even in the MEDW. A likely explanation is that the difference in SI is too small to generate a difference in the depths of the mixed layer. It could however be evidenced that, in the entire MED, MLD-max is always deeper in SAT_VVAR than in SAT_VHOM (see Fig. SM2 in the Supplementary Material) and that the MLD-mean is deeper (up to 50 m deeper) in the MEDW in SAT_VVAR during years of deep and intense convection such as 2009 to 2011 (Fig. 8). This could be explained by the colder upper surface temperature in the SAT_VVAR simulation during the winter season.

5.1.5. An easily avoidable bias

The results clearly show that if the Chl field is vertically homogeneous, a bias will affect the temperature field in the lower surface and intermediate layers. This bias increases over time and would reach significant values after several decades, which corresponds to the scale of long hindcasts or climate projections. This bias introduces an additional but easily avoidable error in the modelled temperatures. Several approaches can be used to generate a 3D Chl field from a 2D surface Chl field, such as the one based on the formulation of Morel and Berthon (1989). This approach is already proposed in the NEMO model (see also Section 5.3 on that point). Here, we propose a new approach to generate a 3D Chl field from a 2D surface Chl field (see Section 2.4). This approach benefits from satellite data, which can be considered more reliable than sea surface model outputs, but also takes advantage of the realistic 3D Chl vertical profiles generated by any biogeochemical model when it has demonstrated its ability to capture most of the spatio-temporal variability of Chl despite its inherent errors. In the present work, we used the biogeochemical model Eco3M-MED, considering that it succeeds in reproducing the main features of Chl variability in the MED (Fig. 4). This 3D Chl field has been used to force the SAT_VVAR simulation.

A Comparison of SAT_VHOM and SAT_VVAR simulations with in situ data was undertaken for the year 2016 (or 2015 when data were too sparse in 2016 as in the case of the Lion buoy), i.e. the last year of the simulation, in order to have maximum differences between the simulations (Fig. 11). This comparison demonstrates the benefit of using a realistic vertical profile of Chl. At both stations in MEDW, the main warm bias in temperature observed in the SAT_VHOM simulation in the lower surface layer is nearly cancelled in the SAT_VVAR simulation, resulting in an improved representation of the summer temperature vertical profile and seasonal thermocline by the model (Fig. 11). In the Levantine basin (MEDE), the cold and warm biases present in SAT_VHOM, respectively in the upper surface and the intermediate layers, are also reduced. The benefit of using realistic vertical variability for Chl is also quantified in the Table 4 where the mean error (bias) and mean absolute error (MAE) between SAT_VVAR and in situ data are significantly lower than for SAT_VHOM (MAE reduced from 4 to more than 70%). However, comparison with the data from the Lion buoy at different seasons shows that, averaged over the year, the errors are a little tighter for all the simulations, although the SAT_VHOM simulation still performs the worst in terms of mean absolute error.

Furthermore, a similar comparison at the scale of the entire Mediterranean basin shows that in all three layers, but especially in the intermediate layer, the temperature calculated with SAT_VVAR is closer to in situ data (see Fig. SM4 in the Supplementary Material).

Finally, although this study focuses on the Mediterranean Sea, it is likely that anywhere in the ocean where Chl is not vertically homogeneous and where DCM is present at least seasonally, the introduction of more realistic vertical variability of Chl, using for example a climatology derived in the same way as in this work, should make it possible to improve the temperature profiles calculated by the ocean circulation model.

5.2. Impact of the temporal frequency of the Chl field

5.2.1. Nature and range of the impact

The influence of the temporal frequency at which the forcing Chl field is saved is another aspect investigated in the present paper. The simulation forced by a daily field (i.e. MOD_DAY) has therefore been compared to the ones respectively forced by climatological (MOD_CLIM) and monthly (MOD_MONTH) Chl fields (see Section 2.4 for more details on the difference between these three simulations). The first aspect to notice is that the temperature differences are smaller than those identified in the previous section on the impact of vertical variability in the Chl field. Moreover, since the climatological Chl field is smoother than the monthly field, the averaged temperature differences

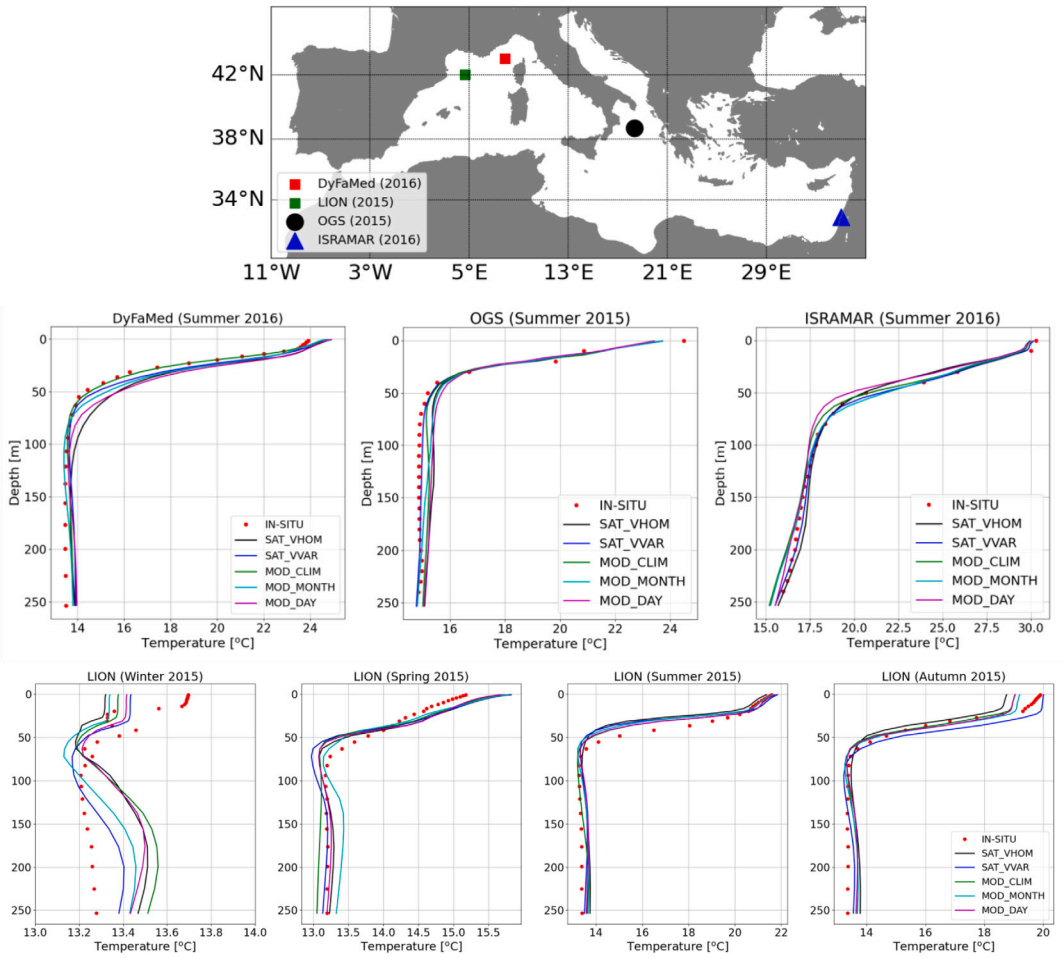

Fig. 11. Comparison of simulated temperature vertical profiles (SAT_VHOM, SAT_VVAR and MOD_CLIM) with in situ data at three different zones in the Mediterranean: DyFaMed site (Coppola et al., 2023) which data are available via the URL: https://www.seanoe.org/data/00326/43749/, Lion buoy site (Bouin, 2011; Bosse et al., 2024), cruise data in the Ionian Sea during June 2015 provided by OGS (https://www.ogs.it/en), and cruise data collected during July 2016 along the southeastern coast and provided by ISRAMAR (https://www.ocean.org.il/en/).

Table 4
Mean Error (ME) and Mean Absolute Error (MAE) of simulations compared to in situ data at the 4 stations shown in Fig. 11.

Simulations	DyFaMed		OGS		IRAMAR		LION	
	ME	MAE	ME	MAE	ME	MAE	ME	MAE
SAT_VHOM	0.039	0.039	0.020	0.024	0.0017	0.014	0.034	0.050
SAT_VVAR	0.025	0.025	0.001	0.007	0.003	0.007	0.045	0.048
MOD_CLIM	0.011	0.013	0.012	0.018	−0.017	0.017	0.035	0.046
MOD_MONTH	0.020	0.022	0.010	0.015	−0.008	0.014	0.037	0.047
MOD_DAY	0.039	0.039	0.019	0.026	−0.020	0.020	0.037	0.047

in absolute value between MOD_CLIM and MOD_DAY (i.e. 0.018°C and 0.01°C respectively in the surface and the intermediate layers) are higher than that between MOD_MONTH and MOD_DAY (Table 3).

Previous work has already studied the impact of using Chl fields of the same nature but with different time frequencies. Ma et al. (2015) and Doi and Behera (2022) compared satellite-derived Chl fields with two different frequencies, namely monthly and annual climatologies. In both cases, the Chl fields used are 2D fields, resulting in changes that mostly affect the surface large-scale dynamics through (moderate) changes in SST. Additionally, Zhang et al. (2018) compared two simulations of the Tropical Pacific forced by the same Chl field provided by an ocean biology model, but either dynamically provided to the ocean model by a biogeochemical model (through a two-way coupling) or provided in the form of a forcing seasonal climatology in the second case. However, they neither focus on the existence of a trend in the temperature difference between the 27-year-long simulations, nor on the temperature difference across the water column.

What is more unexpected in our study is the presence of a trend in the temperature difference between the simulations forced by the same Chl 3D field saved at different temporal frequencies, as evidenced by the Mann–Kendall test (Fig. 10). These trends are of the same sign in the surface and intermediate layers and the opposite sign in the bottom layer due to the feedback of stratification (i.e. a stronger stratification makes the bottom layer more isolated by preventing exchanges with the surface layers and conversely). The fact that ΔT is always negative in the surface and intermediate layers (Fig. 10) and that the trend of ΔT is negative means that the simulation with daily Chl is increasingly warmer than the other two in the surface and especially intermediate

layers. This can also be seen in the vertical profiles shown in Fig. 11, where MOD_DAY temperatures are higher and describe the in situ data surprisingly less well than MOD_MONTH and MOD_CLIM at the end of the simulation (see also Table 4). This could be due to a better error compensation in MOD_MONTH and MOD_CLIM than in MOD_VAR, one of the sources of error being the assumption that all the solar energy absorbed by Chl is transformed to heat, while some is used for photosynthesis.

5.2.2. Why is the temperature higher with a daily chlorophyll forcing?

If the Chl content of the three fields forcing the MOD_DAY, MOD_MONTH and MOD_CLIM simulations is the same on average, the daily chlorophyll field contains more extreme values, i.e. Chl values that are higher or lower than the monthly or the climatological values. In addition, the time interpolation performed by the model on the input forcings will add additional (unrealistic) smoothing, particularly for MOD_CLIM and MOD_MONTH. These peaks of minimum or maximum Chl compensate on average. Still, it seems that their effects on heat accumulation are asymmetrical, preventing them from offsetting each other (Table 3). When the daily Chl is lower, more of the incident irradiance and then more heat reaches the bottom of the surface layer and the top of the intermediate layer, resulting in excess heat in MOD_DAY there. Furthermore, as the surface layer in MOD_DAY is less stratified in this case, the intermediate layer can receive more heat from the surface layer through facilitated exchanges. Overall, the MOD_DAY simulation accumulates more heat in the surface and intermediate layers than the other two simulations.

By contrast, when the daily Chl is higher, the surface water in MOD_DAY is warmer and more stratified, which will potentially affect air-sea heat exchanges as shown in several previous studies (e.g. Oschlies, 2004; Asselot et al., 2022), but restrict exchanges between the surface and the intermediate layers. As a result, the excess heat accumulated in the intermediate layer during the previous episode of low Chl will remain there and be reinforced during subsequent low Chl episodes in MOD_DAY. Consequently, when significant, the trend in ΔT is always negative in the intermediate layer (Fig. 10). It should be noted, however, that in the MEDNW, during years when the mixing is very deep, this excess heat in the intermediate layer is transferred deeper and reaches the bottom layer where ΔT becomes negative while ΔT becomes positive in the intermediate layer.

In conclusion, the source of the temperature differences between simulations does not come directly from the total amount of Chl read by the model, but rather from the differences in the amount of Chl read at each time step and the asymmetrical role of maximal and minimal Chl peaks. Combined with the variability of the physical environment, and in particular solar radiation, which influences the heat balance of seawater at each instant, these differences lead to a gradual warming (cooling) of the surface and intermediate (bottom) layers in the MOD_DAY simulation compared to the MOD_MONTH and MOD_CLIM simulations. These results have however to be confirmed through longer simulations.

5.3. Elements of strategy concerning the choice of Chl fields in ocean models

Using a two-way coupling between a physical model and a (validated) biogeochemical model should be the best way to reduce the potential bias on the heat budget introduced by the absence or the poor representation of biological feedback. It comes however generally at the expense of substantially higher computational costs, which may act as a brake on the exploration of climate projections with timescales of several decades.

To reduce the computational costs associated with long-term projections, a common practice is to dispense with dynamic coupling with a biogeochemical model while replacing the biological feedback on ocean physics with the use of already available Chl forcing fields. In the best cases, these fields are generated by biogeochemical models used in previous simulations, but it is not uncommon for them to be constructed in an extremely simplistic manner.

A large body of literature has already explored the impact of using a Chl field rather than another, mainly as regards the surface temperature and large-scale features. Concerning the vertical shape of the 3D Chl field, several previous studies (Manizza et al., 2005; Hernandez et al., 2017; Gera et al., 2020) relied on the generation of vertical profiles of Chl from the surface value using the formulation of Morel and Berthon (1989). However, this formulation modulates the shape of the vertical profile according to the Chl concentration at the sea surface, without consideration of the physical forcing, the seasonal variations, or the latitude. More problematic is the fact that these vertical Chl profiles are disconnected from the physical environment even though the latter strongly contributes to the control of the depths of the nutriclines and the DCM.

Overall, these previous studies lead to the conclusion that the nature of the forcing Chl field will potentially significantly affect the physics. Solutions must therefore be found to limit the error made by using a forcing Chl field instead of dynamic biogeochemical feedback via a two-way coupling. One such solution is to use data assimilation, as shown by a recent study by Skákala et al. (2022) indicating that, although the two-way coupled model performs slightly better than the one-way coupled model, the difference between the two could become negligible thanks to the assimilation of multi-platform physical data (e.g. temperature, salinity, sea surface height).

An alternative and fruitful approach is the one proposed in this work, namely the construction of a realistic 3D Chl climatology by combining satellite surface Chl data and vertical profile shapes derived from a biogeochemical model (see Section 2.4 for more details on the construction of the Chl 3D climatology), which significantly improves the modelled vertical temperature profiles without considerable effort (see Fig. 11 and Section 5.1.5).

Note that this Chl climatology could also have been derived from a coupled two-way version of the NEMOMED12/Eco3M-MED model instead of the one-way coupling used in the present work. Chl profiles would theoretically have been even more realistic, but we can reasonably assume that they would not have been significantly different since temperature has no direct effect on biogeochemistry in the Eco3M-MED model (i.e. the rates of biogeochemical processes do not depend on temperature). Concerning the indirect effect (i.e. the effect on mixing which also affects biogeochemistry), it should also be very small, since the simulations lasted eleven years, whereas we conclude in this work that the persistent effect on temperature (and probably on biogeochemical quantities) of the use of different Chl fields in the Mediterranean Sea would only be significant after several decades. This assumption should however be verified in future work.

Another aspect to be considered when selecting a forcing 3D Chl field is the time frequency at which concentrations have been saved. Here, 3D forcing Chl fields saved at three different frequencies, namely daily (MOD_DAY), monthly (MOD_MONTH), and monthly climatology (MOD_CLIM), were compared.

The presence of a trend in the temperature difference between MOD_MONTH and MOD_DAY, and mostly between MOD_CLIM and MOD_DAY, that we explained through an asymmetrical role of Chl maximum and minimum (see Section 5.2.2), were rather unexpected. However, these trends are weak, i.e. less than 0.3 °C over 100 years if we extrapolate the trend determined over the 11-year-long period (which is certainly debatable). This, and the fact that MOD_CLIM reproduces the data better than MOD_MONTH and MOD_DAY (see Table 4), suggests that a monthly climatological Chl field can be used as a first approach for long-term simulations. The exploration of scenarios strongly affecting nutrient inputs to the MED should, however, be given particular attention, and may require monthly Chl fields rather than a climatological field. Indeed, strong variations in riverine nutrient inputs over long periods can significantly reshape the biogeochemistry of the Mediterranean, including the nutriclines and the DCM depths, as shown

in Pagès et al. (2020a). Similarly, major changes in the MLD, such as those predicted in the MEDNW by climate projections, should also lead to significant changes in the vertical Chl profiles (Pagès et al., 2020b), making forcing by a climatological Chl no longer appropriate.

6. Conclusion

Climate projections are an essential pillar of the ongoing collective thinking on the future of earth and oceans. The latest (AR6) SSP scenarios provided by IPCC (2023) combine scenarios for greenhouse gas emissions and Socio-Economic (SE) scenarios that are characterized by general guidelines. The quantitative declination of each SE scenario is therefore not unique. For instance, a given SSP scenario may encompass different fishing strategies, agricultural practices, or land use, whose effects on marine ecosystems could be very different.

In this context, there is a real need to explore a sufficient number of scenarios to grasp the envelope of possible pathways. This means producing a sufficiently large number of projections to raise the question of how to reduce computational costs. One of the solutions adopted by physical modellers when coupling the ocean circulation model with a biogeochemical model generates too great a computational overhead is to use a simplistic representation of biogeochemistry via the use of a chlorophyll forcing field, which is not without consequences for the physics calculated by the model, especially if the Chl data in the field are of poor quality.

The aim of this work, which focuses on the Mediterranean Sea, is to analyse the impact on physics (mainly temperature) of using a frequently used Chl forcing field which is composed of realistic surface values (provided by a Chl climatology derived from satellite products), but unrealistic values in the vertical dimension (as it is vertically homogeneous). For comparison purposes, we constructed a Chl climatology using an original method described in this paper. This monthly 3D climatology of Chl benefits both from satellite ocean colour products for the surface field, and from the realism of the Eco3M-MED model for the vertical space–time variability. Eleven-year simulations forced by one or other of these climatologies were compared.

Results first show the important finding that using a vertically homogeneous Chl field results in an artificial heat accumulation below the DCM depth (here around 70 m), which increases with time. Extrapolated over 100 years, the trend associated with this excess heat could lead to a positive temperature bias of up to 1 °C in the intermediate layer, and 0.8 °C in the lower surface layer, which is far from negligible. In addition, no trend could be identified on the difference in MLD between both simulations, but a significant trend was determined for the difference in the stratification index.

Comparison with in situ data showed that using this new Chl field improved the modelled temperature field in the layers mainly affected by this artificial and easily avoidable excess heat. Such a dimensionless climatological 3D field could therefore be an additional option for the NEMO model or any other ocean model.

Finally, the last results of this paper are based on a comparison between simulations using the same 3D Chl field but saved at three different frequencies (i.e. daily, monthly, and monthly climatological). Unexpectedly, the simulation forced by daily Chl turned out to be increasingly warmer in the surface and intermediate layers (and colder in the bottom layer) than the simulations based on a Chl saved at a lower frequency. The proposed explanation lies in the asymmetrical effect on heat accumulation of the maximum and minimum Chl peaks present in the daily Chl field (but less present and less intense in the lower frequency Chl fields). Consequently, their effects do not offset each other on average. Moreover, compared with in situ data, daily Chl forcing did not give better results than monthly or climatological forcing. This could be due to better error compensation in the low-frequency fields, but further research is needed to confirm this assumption. At this stage, monthly-climatological Chl forcing seems suitable as a first approach for physical modelling of the Mediterranean basin, including for long-term projections, bearing in mind however that strong and long-lasting changes in river nutrient inputs and/or in the depth of the mixed layer could have a significantly impact on Chl concentrations and, in particular, on DCM phenology, to such an extent that climatology would no longer be appropriate.

CRediT authorship contribution statement

Yutong Zhang: Writing – original draft, Visualization, Validation, Software, Methodology, Investigation, Data curation. **Florence Sevault:** Writing – original draft, Visualization, Validation, Software, Resources, Investigation, Formal analysis, Data curation. **Romain Pennel:** Writing – original draft, Investigation, Formal analysis. **Melika Baklouti:** Writing – review & editing, Writing – original draft, Supervision, Project administration, Methodology, Investigation, Funding acquisition, Formal analysis, Conceptualization.

Declaration of competing interest

The authors declare that they have no known competing financial interests or personal relationships that could have appeared to influence the work reported in this paper.

Acknowledgements

This work received support (funding of Yutong Zhang's M2 internship) from the French government under the France 2030 investment plan, as part of the Initiative d'Excellence d'Aix-Marseille Université - A*MIDEX - Institute for Ocean Sciences (no AMX-21-IET-016). This study is also a contribution to the MEDIATION PPR-OCEAN project (no ANR-22-POCE-0003) funded by the French Government "France 2030" program of the French National Research Agency (ANR). We acknowledge the MOOSE program (Mediterranean Ocean Observing System for the Environment) coordinated by CNRS-INSU and the Research Infrastructure ILICO (CNRS-IFREMER). We would also like to acknowledge the E.U. Copernicus Marine Service Information for providing access to ocean colour satellite data, and the PERSEUS project (Policy-oriented Marine Environmental Research for the Southern European Seas) for providing access to the in situ temperature and chlorophyll databases in the Mediterranean.

Appendix A. Supplementary data

Supplementary material related to this article can be found online at https://doi.org/10.1016/j.ocemod.2024.102490.

Data availability

Data will be made available on request.

References

Adloff, F., Jordà, G., Somot, S., Sevault, F., Arsouze, T., Meyssignac, B., Li, L., Planton, S., 2018. Improving sea level simulation in mediterranean regional climate models. Clim. Dyn. 51 (3), 1167–1178. http://dx.doi.org/10.1007/s00382-017-3842-3.

Alekseenko, E., Raybaud, V., Espinasse, B., Carlotti, F., Queguiner, B., Thouvenin, B., Garreau, P., Baklouti, M., 2014. Seasonal dynamics and stoichiometry of the planktonic community in the NW Mediterranean sea: a 3D modeling approach. Ocean Dyn. 64, 179–207. http://dx.doi.org/10.1007/s10236-013-0669-2.

Anderson, W., Gnanadesikan, A., Wittenberg, A., 2009. Regional impacts of ocean color on Tropical Pacific variability. Ocean Sci. 5 (3), 313–327. http://dx.doi.org/10.5194/os-5-313-2009.

Arakawa, A., Lamb, V.R., 1981. A potential enstrophy and energy conserving scheme for the shallow water equations. Mon. Weather Rev. 109 (1), 18–36. http://dx.doi.org/10.1175/1520-0493(1981)109<0018:APEAEC>2.0.CO;2.

Asselot, R., Lunkeit, F., Holden, P.B., Hense, I., 2021. The relative importance of phytoplankton light absorption and ecosystem complexity in an earth system model. J. Adv. Model. Earth Syst. 13 (5), e2020MS002110. http://dx.doi.org/10.1029/2020MS002110.

Asselot, R., Lunkeit, F., Holden, P.B., Hense, I., 2022. Climate pathways behind phytoplankton-induced atmospheric warming. Biogeosciences 19 (1), 223–239. http://dx.doi.org/10.5194/bg-19-223-2022.

Baklouti, M., Faure, V., Pawlowski, L., Sciandra, A., 2006. Investigation and sensitivity analysis of a mechanistic phytoplankton model implemented in a new modular numerical tool (Eco3M) dedicated to biogeochemical modelling. Progr. Oceanogr. 71 (1), 34–58. http://dx.doi.org/10.1016/j.pocean.2006.05.003.

Baklouti, M., Pagès, R., Alekseenko, E., Guyennon, A., Grégori, G., 2021. On the benefits of using cell quotas in addition to intracellular elemental ratios in flexible-stoichiometry plankton functional type models. Application to the Mediterranean Sea. Progr. Oceanogr. 197, 102634. http://dx.doi.org/10.1016/j.pocean.2021.102634.

Balmaseda, M.A., Mogensen, K., Weaver, A.T., 2013. Evaluation of the ECMWF ocean reanalysis system ORAS4. Q. J. Royal Meteorol. Soc. 139 (674), 1132–1161.

Barnier, B., Madec, G., Penduff, T., Molines, J.-M., Treguier, A.-M., Le Sommer, J., Beckmann, A., Biastoch, A., Boning, J., Derval, C., Durand, E., Gulev, S., Remy, E., Talandier, C., Theetten, S., Maltrud, M., McClean, J., De Cuevas, B., 2006. Impact of partial steps and momentum advection schemes in a global ocean circulation model at eddy-permitting resolution. Ocean Dyn. 56 (5), 543–567. http://dx.doi.org/10.1007/s10236-006-0082-1.

Berrisford, P., Dee, D., Fielding, K., Fuentes, M., Kallberg, P., Kobayashi, S., Uppala, S., 2009. The ERA-interim archive. ERA Rep. Series (1), 1–16.

Berthet, S., Jouanno, J., Séférian, R., Gehlen, M., Llovel, W., 2023. How does the phytoplankton–light feedback affect the marine N_2O inventory? Earth Syst. Dyn. 14 (2), 399–412. http://dx.doi.org/10.5194/esd-14-399-2023.

Beuvier, J., Lebeaupin Brossier, C., Béranger, K., Arsouze, T., Bourdalle-Badie, R., Deltel, C., Drillet, Y., Drobinski, P., Ferry, N., Lyard, F., Sevault, F., Somot, S., 2012. MED12, oceanic component for the modeling of the regional mediterranean earth system. Mercator Ocean Q. Newslett..

Blanke, B., Delecluse, P., 1993. Variability of the tropical atlantic ocean simulated by a general circulation model with two different mixed-layer physics. J. Phys. Oceanogr. 23 (7), 1363–1388. http://dx.doi.org/10.1175/1520-0485(1993)023<1363:VOTTAO>2.0.CO;2.

Bosse, A., Testor, P., Coppola, L., Bretel, P., Dausse, D., Durrieu de Madron, X., Houpert, L.c., Labaste, M., Legoff, H., Mortier, L., D'ortenzio, F., 2024. LION observatory data. http://dx.doi.org/10.17882/44411.

Bosse, A., Testor, P., Houpert, L.c., Damien, P., Prieur, L., Hayes, D., Taillandier, V., Durrieu de Madron, X., d'Ortenzio, F., Coppola, L., Karstensen, J., Mortier, L., 2016. Scales and dynamics of submesoscale coherent vortices formed by deep convection in the northwestern mediterranean sea. J. Geophys. Res.: Oceans 121 (10), 7716–7742. http://dx.doi.org/10.1002/2016JC012144.

Bouin, M.-N., 2011. 0-250 m ocean temperature, mooring line, lion buoy.

Canova, F., 1998. Detrending and business cycle facts. J. Monetary Econ. 41 (3), 475–512. http://dx.doi.org/10.1016/S0304-3932(98)00006-3.

Colin, J., Déqué, M., Radu, R., Somot, S., 2010. Sensitivity study of heavy precipitation in limited area model climate simulations: influence of the size of the domain and the use of the spectral nudging technique. Tellus A: Dyn. Meteorol. Oceanogr. 62 (5), 591–604. http://dx.doi.org/10.1111/j.1600-0870.2010.00467.x.

Coppola, L., Diamond Riquier, E., Carval, T., Irisson, J.-O., Desnos, C., 2023. Dyfamed observatory data. http://dx.doi.org/10.17882/43749.

Courtois, P., Hu, X., Pennelly, C., Spence, P., Myers, P.G., 2017. Mixed layer depth calculation in deep convection regions in ocean numerical models. Ocean Model. 120, 60–78. http://dx.doi.org/10.1016/j.ocemod.2017.10.007.

Craig, A., Valcke, S., Coquart, L., 2017. Development and performance of a new version of the OASIS coupler, OASIS3-MCT_3.0. Geosci. Model Develop. 10 (9), 3297–3308. http://dx.doi.org/10.5194/gmd-10-3297-2017.

Darmaraki, S., Somot, S., Sevault, F., Nabat, P., 2019. Past variability of Mediterranean Sea marine heatwaves. Geophys. Res. Lett. 46 (16), 9813–9823. http://dx.doi.org/10.1029/2019GL082933.

Decharme, B., Delire, C., Minvielle, M., Colin, J., Vergnes, J.-P., Alias, A., Saint-Martin, D., Séférian, R., Sénési, S., Voldoire, A., 2019. Recent changes in the ISBA-CTRIP land surface system for use in the CNRM-CM6 climate model and in global off-line hydrological applications. J. Adv. Model. Earth Syst. 11 (5), 1207–1252. http://dx.doi.org/10.1029/2018MS001545.

Doi, T., Behera, S., 2022. Impacts of interannual variations of chlorophyll on seasonal predictions of the tropical Pacific. Front. Climate 4, http://dx.doi.org/10.3389/fclim.2022.868594.

Doney, S.C., Ruckelshaus, M., Emmett Duffy, J., Barry, J.P., Chan, F., English, C.A., Galindo, H.M., Grebmeier, J.M., Hollowed, A.B., Knowlton, N., Polovina, J., Rabalais, N.N., Sydeman, W.J., Talley, L.D., 2012. Climate change impacts on marine ecosystems. Annual Rev. Marine Sci. 4, 11–37. http://dx.doi.org/10.1146/annurev-marine-041911-111611.

Durrieu de Madron, X., Guieu, C., Sempéré, R., Conan, P., Cossa, D., D'Ortenzio, F., Estournel, C., Gazeau, F., Rabouille, C., Stemmann, L., Bonnet, S., Diaz, F., Koubbi, P., Radakovitch, O., Babin, M., Baklouti, M., Bancon-Montigny, C., Belviso, S., Bensoussan, N., Bonsang, B., Bouloubassi, I., Brunet, C., Cadiou, J.F., Carlotti, F., Chami, M., Charmasson, S., Charrière, B., Dachs, J., Doxaran, D., Dutay, J.C., Elbaz-Poulichet, F., Eléaume, M., Eyrolles, F., Fernandez, C., Fowler, S., Francour, P., Gaertner, J.C., Galzin, R., Gasparini, S., Ghiglione, J.F., Gonzalez, J.L., Goyet, C., Guidi, L., Guizien, K., Heimbürger, L.E., Jacquet, S.H., Jeffrey, W.H., Joux, F., Le Hir, P., Leblanc, K., Lefèvre, D., Lejeusne, C., Lemé, R., Loÿe-Pilot, M.D., Mallet, M., Méjanelle, L., Mélin, F., Mellon, C., Mérigot, B., Merle, P.L., Migon, C., Miller, W.L., Mortier, L., Mostajir, B., Mousseau, L., Moutin, T., Para, J., Pérez, T., Petrenko, A., Poggiale, J.C., Prieur, L., Pujo-Pay, M., Pulido-Villena, Raimbault, P., Rees, A.P., Ridame, C., Rontani, J.F., Ruiz Pino, D., Sicre, M.A., Taillandier, V., Tamburini, C., Tanaka, T., Taupier-Letage, I., Tedetti, M., Testor, P., Thébault, H., Thouvenin, B., Touratier, F., Tronczynski, J., Ulses, C., Van Wambeke, F., Vantrepotte, V., Vaz, S., Verney, R., 2011. Marine ecosystems' responses to climatic and anthropogenic forcings in the mediterranean. Prog. Oceanogr. 91 (2), 97–166. http://dx.doi.org/10.1016/j.pocean.2011.02.003.

Flato, G.M., 2011. Earth system models: an overview. WIREs Climate Change 2 (6), 783–800. http://dx.doi.org/10.1002/wcc.148.

Frouin, R., Ueyoshi, K., Kampel, M., 2007. Influence of solar radiation absorbed by phytoplankton on the thermal structure and circulation of the tropical Atlantic Ocean. In: Proceedings of SPIE - the International Society for Optical Engineering, vol. 6680. pp. 324–335. http://dx.doi.org/10.1117/12.738969.

Gattuso, J.-P., Magnan, A.K., Bopp, L., Cheung, W.W.L., Duarte, C.M., Hinkel, J., Mcleod, E., Micheli, F., Oschlies, A., Williamson, P., Billé, R., Chalastani, V.I., Gates, R.D., Irisson, J.-O., Middelburg, J.J., Pörtner, H.-O., Rau, G.H., 2018. Ocean solutions to address climate change and its effects on marine ecosystems. Front. Marine Sci. 5, 337. http://dx.doi.org/10.3389/fmars.2018.00337.

Gehlen, M., Barciela, R., Bertino, L., Brasseur, P., Butenschön, M., Chai, F., Crise, A., Drillet, Y., Ford, D., Lavoie, D., Lehodey, P., Perruche, C., Samuelsen, A., Simon, E., 2015. Building the capacity for forecasting marine biogeochemistry and ecosystems: recent advances and future developments. J. Oper. Oceanogr. 8 (sup1), s168–s187. http://dx.doi.org/10.1080/1755876X.2015.1022350.

Gera, A., Mitra, A.K., McCreary, J.P., Hood, R., Momin, I.M., 2020. Impact of chlorophyll concentration on thermodynamics and dynamics in the tropical Indian ocean. Deep Sea Res. II: Top. Stud. Oceanogr. 179, 104871. http://dx.doi.org/10.1016/j.dsr2.2020.104871.

Gnanadesikan, A., Anderson, W.G., 2009. Ocean water clarity and the ocean general circulation in a coupled climate model. J. Phys. Oceanogr. 39 (2), 314–332. http://dx.doi.org/10.1175/2008JPO3935.1.

Guyennon, A., Baklouti, M., Diaz, F., Palmieri, J., Beuvier, J., Lebaupin-Brossier, C., Arsouze, T., Béranger, K., Dutay, J.C., Moutin, T., 2015. New insights into the organic carbon export in the [mediterranean] Sea from 3D modeling. Biogeosciences 12, 7025–7046. http://dx.doi.org/10.5194/bg-12-7025-2015.

Hamon, M., Beuvier, J., Somot, S., Lellouche, J., Greiner, E., Jordà, G., Bouin, M., Arsouze, T., Béranger, K., Sevault, F., Dubois, C., Drevillon, M., Drillet, Y., 2016. Design and validation of MEDRYS, a Mediterranean Sea reanalysis over 1992–2013. Ocean Sci. Discuss. 12 (2), http://dx.doi.org/10.5194/os-12-577-2016.

Hernandez, O., Jouanno, J., Echevin, V., Aumont, O., 2017. Modification of sea surface temperature by chlorophyll concentration in the atlantic upwelling systems. J. Geophys. Res. Oceans 122 (7), 5367–5389. http://dx.doi.org/10.1002/2016JC012330.

Hirsch, R.M., Slack, J.R., Smith, R.A., 1982. Techniques of trend analysis for monthly water quality data. Water Resour. Res. 18 (1), 107–121. http://dx.doi.org/10.1029/WR018i001p00107.

Hoegh-Guldberg, O., Bruno, J.F., 2010. The impact of climate change on the world's marine ecosystems. Science 328 (5985), 1523–1528. http://dx.doi.org/10.1126/science.1189930.

IPCC, 2023. Climate Change 2023: Synthesis Report. *Contribution of Working Groups I, II and III to the Sixth Assessment Report of the Intergovernmental Panel on Climate Change*. Technical Report, IPCC, Geneva, Switzerland.

Lengaigne, M., Menkes, C., Aumont, O., Gorgues, T., Bopp, L., André, J.-M., Madec, G., 2007. Influence of the oceanic biology on the tropical Pacific climate in a coupled general circulation model. Climate Dyn. 28, 503–516. http://dx.doi.org/10.1007/s00382-006-0200-2.

Lewis, M.R., Cullen, J.J., Platt, T., 1983. Phytoplankton and thermal structure in the upper ocean: consequences of nonuniformity in chlorophyll profile. J. Geophys. Res. Oceans 88 (C4), 2565–2570. http://dx.doi.org/10.1029/JC088iC04p02565.

Lin, P., Liu, H., Zhang, X., 2008. Effect of chlorophyll-a spatial distribution on upper ocean temperature in the central and Eastern Equatorial Pacific. Adv. Atmospher. Sci. 25, 585–596. http://dx.doi.org/10.1007/s00376-008-0585-4.

Lionello, P., Scarascia, L., 2018. The relation between climate change in the mediterranean region and global warming. Regional Environ. Change 18, 1481–1493. http://dx.doi.org/10.1007/s10113-018-1290-1.

Löptien, U., Eden, C., Timmermann, A., Dietze, H., 2009. Effects of biologically induced differential heating in an eddy-permitting coupled ocean-ecosystem model. J. Geophys. Res. Oceans 114 (C6), http://dx.doi.org/10.1029/2008JC004936.

Ma, J., Liu, H., Lin, P., Zhan, H., 2015. Effects of the interannual variability in chlorophyll concentrations on sea surface temperatures in the east tropical Indian ocean. J. Geophys. Res. Oceans 120 (10), 7015–7027. http://dx.doi.org/10.1002/2015JC010862.

Macias, D.M., Garcia-Gorriz, E., Stips, A., 2015. Productivity changes in the mediterranean sea for the twenty-first century in response to changes in the regional atmospheric forcing. Front. Marine Sci. 2, 79. http://dx.doi.org/10.3389/fmars.2015.00079.

Madec, G., Bell, M., Blaker, A., Bricaud, C., Bruciaferri, D., Castrillo, M., Calvert, D., Chanut, J., Clementi, E., Coward, A., Epicoco, I., Éthé, C., Ganderton, J., Harle, J., Hutchinson, K., Iovino, D., Lea, D., Lovato, T., Martin, M., Martin, N., Mele, F., Martins, D., Masson, S., Mathiot, P., Mele, F., Mocavero, S., Müller, S., Nurser, A.G., Paronuzzi, S., Peltier, M., Person, R., Rousset, C., Rynders, S., Samson, G., Téchené, S., Vancoppenolle, M., Wilson, C., 2023. NEMO ocean engine reference manual. http://dx.doi.org/10.5281/zenodo.8167700.

Malanotte-Rizzoli, P., Artale, V., Borzelli-Eusebi, G.L., Brenner, S., Crise, A., Gacic, M., Kress, N., Marullo, S., Ribera d'Alcalà, M., Sofianos, S., Tanhua, T., Theocharis, A., Alvarez, M., Ashkenazy, Y., Bergamasco, A., Cardin, V., Carniel, S., Civitarese, G., D'Ortenzio, F., Font, J., Garcia-Ladona, E., Garcia-Lafuente, J.M., Gogou, A., Gregoire, M., Hainbucher, D., Kontoyannis, H., Kovacevic, V., Kraskapoulou, E., Kroskos, G., Incarbona, A., Mazzocchi, M.G., Orlic, M., Ozsoy, E., Pascual, A., Poulain, P.-M., Roether, W., Rubino, A., Schroeder, K., Siokou-Frangou, J., Souvermezoglou, E., Sprovieri, M., Tintoré, J., Triantafyllou, G., 2014. Physical forcing and physical/biochemical variability of the mediterranean sea: a review of unresolved issues and directions for future research. Ocean Sci. 10 (3), 281–322. http://dx.doi.org/10.5194/os-10-281-2014.

Malanotte-Rizzoli, P., Manca, B.B., d'Alcala, M.R., Theocharis, A., Brenner, S., Budillon, G., Ozsoy, E., 1999. The eastern mediterranean in the 80s and in the 90s: the big transition in the intermediate and deep circulations. Dyn. Atmos. Oceans 29 (2), 365–395. http://dx.doi.org/10.1016/S0377-0265(99)00011-1.

Manizza, M., Le Quéré, C., Watson, A.J., Buitenhuis, E.T., 2005. Bio-optical feedbacks among phytoplankton, upper ocean physics and sea-ice in a global model. Geophys. Res. Lett. 32 (5), http://dx.doi.org/10.1029/2004GL020778.

Manizza, M., Le Quéré, C., Watson, A.J., Buitenhuis, E.T., 2008. Ocean biogeochemical response to phytoplankton-light feedback in a global model. J. Geophys. Res. Oceans 113 (C10), http://dx.doi.org/10.1029/2007JC004478.

Mann, H., 1945. Non-parametric tests against trend. Econometria http://dx.doi.org/10.2307/1907187.

Mason, E., Barceló-Llull, B., Sànchez-Román, A., Rodríguez-Tarry, D., Cutolo, E., Delepoulle, A., Ruiz, S., Pascual, A., 2023. Chapter 8 - fronts, eddies and mesoscale circulation in the mediterranean sea. In: Schroeder, K., Chiggiato, J. (Eds.), Oceanography of the Mediterranean Sea. Elsevier, pp. 263–287. http://dx.doi.org/10.1016/B978-0-12-823692-5.00003-0.

Melis, A., 2009. Solar energy conversion efficiencies in photosynthesis: minimizing the chlorophyll antennae to maximize efficiency. Plant Sci. 177 (4), 272–280. http://dx.doi.org/10.1016/j.plantsci.2009.06.005.

Menon, S., Denman, K., Brasseur, G., Chidthaisong, A., Ciais, P., Cox, P., Dickinson, R., Hauglustaine, D., Heinze, C., Holland, E., Jacob, D., Lohmann, U., Ramachandran, S., Silva Dias, P., Wofsy, S., Zhang, X., 2007. Couplings between changes in the climate system and biogeochemistry. pp. 499–587.

Millot, C., Taupier-Letage, I., 2005. Circulation in the Mediterranean Sea. In: The Handbook of Environmental Chemistry, vol. K. pp. 29–66. http://dx.doi.org/10.1007/b107143.

Morel, A., 1988. Optical modeling of the upper ocean in relation to its biogenous matter content (case I waters). J. Geophys. Res. Oceans 93 (C9), 10749–10768. http://dx.doi.org/10.1029/JC093iC09p10749.

Morel, A., Berthon, J.-F., 1989. Surface pigments, algal biomass profiles, and potential production of the euphotic layer: relationships reinvestigated in view of remote-sensing applications. Limnol. Oceanogr. 34 (8), 1545–1562. http://dx.doi.org/10.4319/lo.1989.34.8.1545.

Morel, A., Maritorena, S., 2001. Bio-optical properties of oceanic waters: a reappraisal. J. Geophys. Res. Oceans 106 (C4), 7163–7180. http://dx.doi.org/10.1029/2000JC000319.

Moullec, F., Barrier, N., Drira, S., Guilhaumon, F., Marsaleix, P., Somot, S., Ulses, C., Velez, L., Shin, Y.-J., 2019. An end-to-end model reveals losers and winners in a warming Mediterranean Sea. Front. Marine Sci. 6, http://dx.doi.org/10.3389/fmars.2019.00345.

Moutin, T., Van Wambeke, F., Prieur, L., 2012. Introduction to the biogeochemistry from the oligotrophic to the ultraoligotrophic mediterranean (BOUM) experiment. Biogeosciences 9 (10), 3817–3825. http://dx.doi.org/10.5194/bg-9-3817-2012.

Nabat, P., Somot, S., Cassou, C., Mallet, M., Michou, M., Bouniol, D., Decharme, B., Drugé, T., Roehrig, R., Saint-Martin, D., 2020. Modulation of radiative aerosols effects by atmospheric circulation over the euro-mediterranean region. Atmospher. Chem. Phys. 20 (14), 8315–8349. http://dx.doi.org/10.5194/acp-20-8315-2020.

Nakamoto, S., Kumar, S.P., Oberhuber, J., Ishizaka, J., Muneyama, K., Frouin, R., 2001. Response of the Equatorial Pacific to chlorophyll pigment in a mixed layer isopycnal ocean general circulation model. Geophys. Res. Lett. 28 (10), 2021–2024. http://dx.doi.org/10.1029/2000GL012494.

Nakamoto, S., Kumar, S.P., Oberhuber, J.M., Muneyama, K., Frouin, R., 2000. Chlorophyll modulation of sea surface temperature in the Arabian sea in a mixed-layer isopycnal general circulation model. Geophys. Res. Lett. 27 (6), 747–750. http://dx.doi.org/10.1029/1999GL002371.

Oschlies, A., 2004. Feedbacks of biotically induced radiative heating on upper-ocean heat budget, circulation, and biological production in a coupled ecosystem-circulation model. J. Geophys. Res.: Oceans 109 (C12), http://dx.doi.org/10.1029/2004JC002430.

Pagès, R., Baklouti, M., Barrier, N., Ayache, M., Sevault, F., Somot, S., Moutin, T., 2020b. Projected effects of climate-induced changes in hydrodynamics on the biogeochemistry of the Mediterranean Sea under the RCP 8.5 regional climate scenario. Front. Marine Sci. 7, 563615. http://dx.doi.org/10.3389/fmars.2020.563615.

Pagès, R., Baklouti, M., Barrier, N., Richon, C., Dutay, J.-C., Moutin, T., 2020a. Changes in rivers inputs during the last decades significantly impacted the biogeochemistry of the eastern mediterranean basin: A modelling study. Progr. Oceanogr. 181, 102242. http://dx.doi.org/10.1016/j.pocean.2019.102242.

Park, J.-Y., Kug, J.-S., 2014. Marine biological feedback associated with Indian Ocean Dipole in a coupled ocean/biogeochemical model. Climate dynamics 42, 329–343. http://dx.doi.org/10.1007/s00382-012-1640-5.

Park, J.-Y., Stock, C.A., Dunne, J.P., Yang, X., Rosati, A., 2019. Seasonal to multiannual marine ecosystem prediction with a global Earth system model. Science 365 (6450), 284–288. http://dx.doi.org/10.1126/science.aav6634.

Patara, L., Vichi, M., Masina, S., Fogli, P.G., Manzini, E., 2012. Global response to solar radiation absorbed by phytoplankton in a coupled climate model. Climate Dyn. 39 (7–8), 1951–1968. http://dx.doi.org/10.1007/s00382-012-1300-9.

Pearson, K., 1909. Determination of the coefficient of correlation. Science 30 (757), 23–25. http://dx.doi.org/10.1126/science.30.757.23.

Pinardi, N., Auclair, F., Cesarini, C., Demirov, E., Umani, S.F., Giani, M., Montanari, G., Oddo, P., Tonani, M., Zavatarelli, M., 2002. Toward marine environmental predictions in the mediterranean sea coastal areas: a monitoring approach. Ocean Forecasting: Concept. Basis Appl. 339–376. http://dx.doi.org/10.1007/978-3-662-22648-3_17.

Rabinowitch, E.I., 1965. The role of chlorophyll in photosynthesis. Sci. Am. 213 (1), 74–83. http://dx.doi.org/10.1038/scientificamerican0765-74.

Randall, D.A., Bitz, C.M., Danabasoglu, G., Denning, A.S., Gent, P.R., Gettelman, A., Griffies, S.M., Lynch, P., Morrison, H., Pincus, R., Thuburn, J., 2018. 100 years of earth system model development. Meteorol. Monogr. 59, 12.1 – 12.66. http://dx.doi.org/10.1175/AMSMONOGRAPHS-D-18-0018.1.

Robinson, A., Golnaraghi, M., Leslie, W., Artegiani, A., Hecht, A., Lazzoni, E., Michelato, A., Sansone, E., Theocharis, A., Ünlüata, Ü., 1991. The eastern mediterranean general circulation: features, structure and variability. Dyn. Atmospher. Oceans 15 (3–5), 215–240. http://dx.doi.org/10.1016/0377-0265(91)90021-7.

Ruti, P.M., Somot, S., Giorgi, F., Dubois, C., Flaounas, E., Obermann, A., Dell'Aquila, A., Pisacane, G., Harzallah, A., Lombardi, E., Ahrens, B., Akhtar, N., Alias, A., Arsouze, T., Aznar, R., Bastin, S., Bartholy, J., Béranger, K., Beuvier, J., Bouffies-Cloché, S., Brauch, J., Cabos, W., Calmanti, S., Calvet, J.-C., Carillo, A., Conte, D., Coppola, E., Djurdjevic, V., Drobinski, P., Elizalde-Arellano, A., Gaertner, M., Galàn, P., Gallardo, C., Gualdi, S., Goncalves, M., Jorba, O., Jordà, G., L'Heveder, B., Lebeaupin-Brossier, C., Li, L., Liguori, G., Lionello, P., Maciàs, D., Nabat, P., Önol, B., Raikovic, B., Ramage, K., Sevault, F., Sannino, G., Struglia, M.V., Sanna, A., Torma, C., Vervatis, V., 2016. MED-CORDEX initiative for mediterranean climate studies. Bull. Am. Meteorol. Soc. 97 (7), 1187–1208. http://dx.doi.org/10.1175/BAMS-D-14-00176.1.

Sen, P.K., 1968. Estimates of the regression coefficient based on Kendall's tau. J. Am. Statist. Assoc. 63 (324), 1379–1389. http://dx.doi.org/10.2307/2285891.

Sevault, F., 2024. Atlas of the 1980–2018 ERA-interim simulation with the coupled regional climate system model CNRM-RCSM6 (version v2). http://dx.doi.org/10.5281/zenodo.11066601.

Siokou Frangou, I., Christaki, U., Mazzocchi, M., Montresor, M., Ribera d'Alcala, M., Vaque, D., Zingone, A., 2010. Plankton in the open mediterranean sea. a review. Biogeosciences 7, 1543–1586. http://dx.doi.org/10.5194/bg-7-1543-2010.

Skákala, J., Bruggeman, J., Ford, D., Wakelin, S., Akpınar, A., Hull, T., Kaiser, J., Loveday, B.R., O'Dea, E., Williams, C.A., Williams, Ciavatta, S., 2022. The impact of ocean biogeochemistry on physics and its consequences for modelling shelf seas. Ocean Model. 172, 101976. http://dx.doi.org/10.1016/j.ocemod.2022.101976.

Somot, S., 2005. Modélisation climatique du bassin méditerranéen: variabilité et scénarios de changement climatique (Ph.D. thesis). Université Paul Sabatier - Toulouse III.

Somot, S., Houpert, L., Sevault, F., Testor, P., Bosse, A.e.a., 2018. Characterizing, modelling and understanding the climate variability of the deep water formation in the north-western mediterranean sea. Clim. Dyn. 51, 1179–1210. http://dx.doi.org/10.1007/s00382-016-3295-0.

Soto-Navarro, J., Jordá, G., Amores, A., Cabos, W., Somot, S., Sevault, F., Macías, D., Djurdjevic, V., Sannino, G., Li, L., Sein, D., 2020. Evolution of mediterranean sea water properties under climate change scenarios in the med-CORDEX ensemble. Climate Dyn. 54, 2135–2165. http://dx.doi.org/10.1007/s00382-019-05105-4.

Stuart, A., 1956. Rank correlation methods. By M. G. Kendall, 2nd edition. Br. J. Statist. Psychol. 9 (1), 68. http://dx.doi.org/10.1111/j.2044-8317.1956.tb00172.x.

Tian, F., Zhang, R.-H., Wang, X., 2021. Coupling ocean–atmosphere intensity determines ocean chlorophyll-induced SST change in the tropical Pacific. Climate Dyn. 56, 3775–3795. http://dx.doi.org/10.1007/s00382-021-05666-3.

Voldoire, A., Saint-Martin, D., Sénési, S., Decharme, B., Alias, A., Chevallier, M., Colin, J., Guérémy, J.-F., Michou, M., Moine, M.-P., Nabat, P., Roehrig, R., Salas y Mélia, D., Séférian, R., Valcke, S., Beau, I., Belamari, S., Berthet, S., Cassou, C., Cattiaux, J., Deshayes, J., Douville, H., Ethé, C., Franchistéguy, L., Geoffroy, O., Lévy, C., Madec, G., Meurdesoif, Y., Msadek, R., Ribes, A., Sanchez-Gomez, E., Terray, L., Waldman, R., 2019. Evaluation of CMIP6 deck experiments with CNRM-CM6-1. J. Adv. Model. Earth Syst. 11 (7), 2177–2213. http://dx.doi.org/10.1029/2019MS001683.

Waldman, R., Brüggemann, N., Bosse, A., Spall, M., Somot, S., Sevault, F., 2018a. Overturning the mediterranean thermohaline circulation. Geophys. Res. Lett. 45 (16), 8407–8415. http://dx.doi.org/10.1029/2018GL078502.

Waldman, R., Somot, S., Herrmann, M., Sevault, F., Isachsen, P.E., 2018b. On the chaotic variability of deep convection in the mediterranean sea. Geophys. Res. Lett. 45 (5), 2433–2443. http://dx.doi.org/10.1002/2017GL076319.

Waldman, R., Somot, S., Herrmann, M., Testor, P., Estournel, C., Sevault, F., Prieur, L., Mortier, L., Coppola, L., Taillandier, V., Conan, P., Dausse, D., 2016. Estimating dense water volume and its evolution for the year 2012–2013 in the northwestern mediterranean sea: An observing system simulation experiment approach. J. Geophys. Res. Oceans 121 (9), 6696–6716. http://dx.doi.org/10.1002/2016JC011694.

Wetzel, P., Maier-Reimer, E., Botzet, M., Jungclaus, J., Keenlyside, N., Latif, M., 2006. Effects of ocean biology on the penetrative radiation in a coupled climate model. J. Clim. 19 (16), 3973–3987. http://dx.doi.org/10.1175/JCLI3828.1.

Wright, L., Davidson, S., 2020. How to tell the difference between a model and a digital twin. Adv. Model. Simul. Eng. Sci. 7 (1), 1–13. http://dx.doi.org/10.1186/s40323-020-00147-4.

Zhang, R.-H., Tian, F., Wang, X., 2018. Ocean chlorophyll-induced heating feedbacks on ENSO in a coupled ocean physics–biology model forced by prescribed wind anomalies. J. Climate 31 (5), 1811–1832. http://dx.doi.org/10.1175/JCLI-D-17-0505.1.